The Akato Tagh bend along the Altyn Tagh fault, northwest Tibet 1: Smoothing by vertical-axis rotation and the effect of topographic stresses on bend-flanking faults

Eric Cowgill†
An Yin
Department of Earth and Space Sciences, University of California, Los Angeles, California 90095, USA

J Ramón Arrowsmith
Department of Geological Sciences, Arizona State University, Tempe, Arizona 85287, USA

Wang Xiao Feng
Zhang Shuanhong
Institute of Geomechanics, Chinese Academy of Geological Sciences, Beijing, China

ABSTRACT

To better understand the mechanics of restraining double bends and the strike-slip faults in which they occur, we investigated the relationship between topography and bedrock structure within the Akato Tagh, the largest restraining double bend along the active, left-slip Altyn Tagh fault. The bend comprises a ~90-km long, east-west striking central fault segment flanked by two N70°E-striking sections that parallel the regional strike of the Altyn Tagh system. The three segments form two inside corners in the southwest and northeast sectors of the uplift where they link. We find that both the topography and bedrock structure of the Akato Tagh restraining bend are strongly asymmetric. The highest and widest parts of the uplift are focused into two topographic nodes, one in each inside corner of the bend. Structural mapping of the western half of the bend suggests the southwest node coincides with a region of anomalously high, bend-perpendicular shortening. We also find that partitioned, transpressional deformation within the Akato Tagh borderlands is absorbed by bend-parallel strike-slip faulting and bend-perpendicular folding, unlike the thrusting reported from many other double bends. Synthesis of these results leads to three implications of general significance. First, we show that focusing of bend-perpendicular shortening into the two inside corners of a restraining double bend may cause both the bend and the fault to undergo vertical-axis rotation, thereby reducing the bend angle and smoothing the trace during progressive deformation. Such vertical-axis rotation may help explain why fault trace complexity is inversely related to total displacement along strike-slip faults. Second, we calculate four independent age estimates for the Akato Tagh bend, all of which are much younger than the Altyn Tagh system. We use these estimates in a companion study to postulate that the Altyn Tagh and similarly multi-stranded strike-slip systems may evolve by net strain hardening. Third, comparison of the Akato Tagh with other restraining double bends highlights systematic differences in the style of borderland faulting and we speculate that these variations result from different states of stress adjacent to the bends. Strike-slip dominated bends such as the Akato Tagh may form where $\sigma_H = \sigma_1$, $\sigma_v = \sigma_2$, and $\sigma_h = \sigma_3$ whereas thrust-dominated bends like the Santa Cruz bend along the San Andreas fault form when $\sigma_H = \sigma_1$, $\sigma_h = \sigma_2$, $\sigma_v = \sigma_3$. This hypothesis predicts that the style of faulting along a restraining double bend can evolve during progressive deformation, and we show that either weakening of borderland faults or growth of restraining bend topography can convert thrust-dominated bends into strike-slip dominated uplifts such as the Akato Tagh.

Keywords: restraining bend, Altyn Tagh fault, strike-slip systems, Tibetan Plateau, fault strength, topographic stress.

INTRODUCTION

The active, left-lateral Altyn Tagh fault system (Fig. 1) (Molnar and Tapponnier, 1975, 1978; Tapponnier and Molnar, 1977) is the largest strike-slip fault system within the Indo-Asian collision zone and is thought to have played a central role in accommodating India's ongoing indentation into Eurasia (Peltzer and Tapponnier, 1988). Although active deformation is concentrated along one principal trace, the Altyn Tagh fault, this trace is flanked by a distributed set of secondary strike-slip and oblique-slip structures (Fig. 1) (Cowgill et al., 2000; Jolivet et al., 2001; Liu, 1988; Xinjiang Bureau of Geology and Mineral Resources, 1993). Thus, the Altyn Tagh system constitutes a northeast-striking left-lateral shear zone that is at least 100 km wide (Cowgill et al., 2003; Jolivet et al., 2001). Although several major strike-slip systems are characterized by similarly broad zones of faulting, it remains unclear how these zones evolve during progressive deformation and what this evolution implies about the mechanical behavior of the continental lithosphere. In particular, does the breadth of these zones increase during progressive deformation, and if so, does this expansion indicate that the continental lithosphere deforms by strain-hardening processes (Cowgill et al., 2004; also see Holdsworth et al., 2001)?

Between 85°E and 95°E longitude, the principal active trace of the Altyn Tagh system constitutes an en échelon set of five, northeast-striking straight fault sections punctuated by four shorter, right-stepping, east-west trending

†Present address: Department of Geology, University of California, Davis, California 95616, USA; e-mail: cowgill@geology.ucdavis.edu.

GSA Bulletin; November/December 2004; v. 116; no. 11/12; p. 1423–1442; doi: 10.1130/B25359.1; 12 figures.

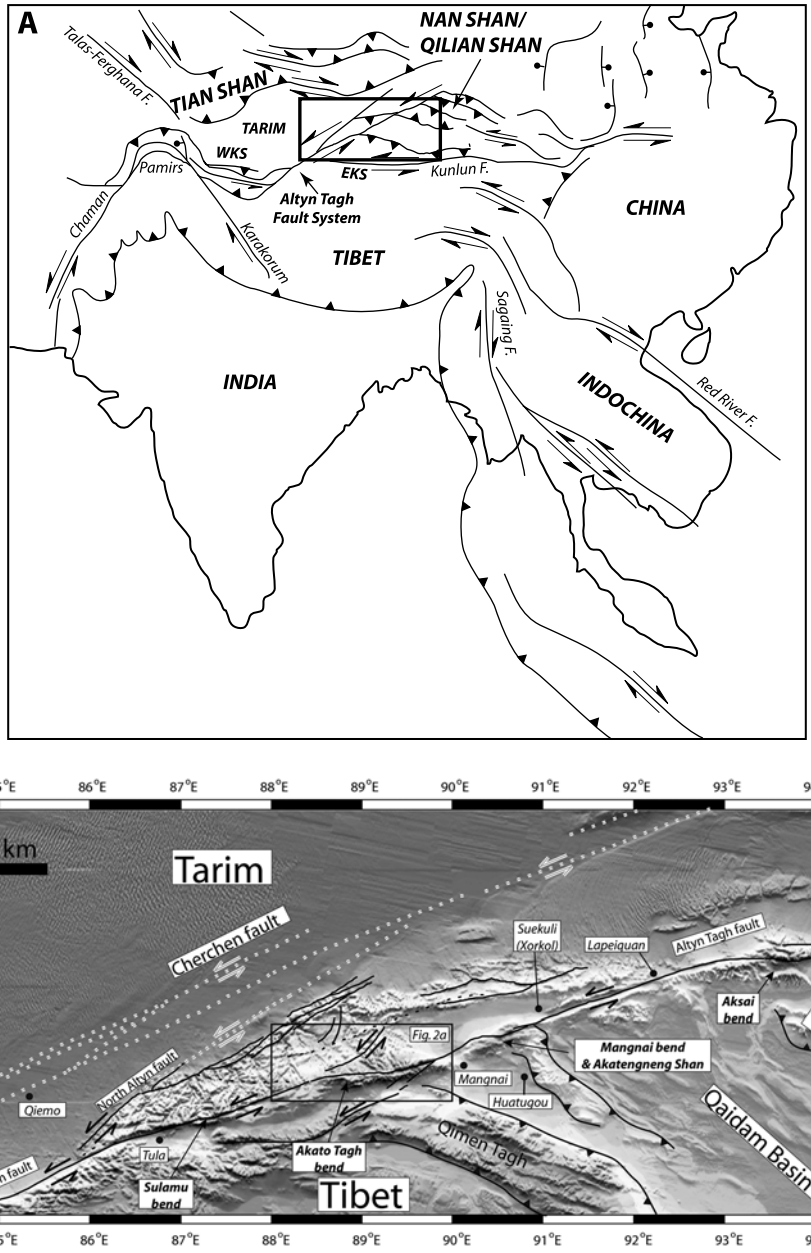

Figure 1. Location of the Akato Tagh restraining double bend along the Altyn Tagh fault within the Indo-Asian collision zone. (A) Simplified map of major faults in the Indo-Asian collision zone. Box outlines Figure 1B. (B) Shaded relief image of the central Altyn Tagh range. Known and inferred strands within the Cenozoic Altyn Tagh fault system as compiled from our mapping and interpretation of CORONA satellite imagery along with previous reports (Chinese State Bureau of Seismology, 1992; Cowgill et al., 2000; Liu, 1988; Meyer et al., 1998). Active trace of the Altyn Tagh fault has four restraining double bends (Sulamu Tagh, Akato Tagh, Akatengneng Shan, and Aksai). Locations of the prominent mountain ranges Eastern and Western Kunlun Shan (EKS and WKS) are shown. Box outlines Figure 2. Base map was generated from the GTOPO30 1 km digital elevation data using GMT software developed by Wessel and Smith (1991).

segments in the Sulamu Tagh, Akato Tagh, Mangnai, and Aksai regions (Fig. 1B). We follow Crowell (1974) in referring to such geometric complexities as *restraining double bends* because the fault trace bends first to the right and then to the left when followed along strike. Because the straight segments are systematically right stepping, there are no releasing double bends of equivalent size to the transpressional jogs along the Altyn Tagh fault. Flanking each restraining double bend are mountain ranges that are anomalously high relative to the surrounding regions (Figs. 1B and 2), suggesting that the double bends are localized sites of active horizontal shortening and rock uplift.

Restraining double bends such as those along the Altyn Tagh fault are key features along strike-slip faults because fault-parallel motion outside the bend produces convergence within the double bend (e.g., Crowell, 1974). Thus, analysis of the amount and timing of deformation within the bend will yield insight into the history of strike-slip faulting along the adjacent fault segments. Bends and stepovers are also thought to exert a first-order control on the initiation and extent of earthquake ruptures (e.g., Du and Aydin, 1995 and references therein; Nielsen and Knopoff, 1998; Segall and Pollard, 1980; Wesnousky, 1988). In this study and a companion paper (Cowgill et al., 2004) we present an integrated bedrock and neotectonic investigation of the 90 km-long Akato Tagh range, the largest double restraining bend along the Altyn Tagh fault. Cowgill et al. (2004) investigates the age of the active trace relative to the Altyn Tagh system as a whole to explore the question of whether or not strain hardening is important in producing geometrically complex, multi-stranded strike-slip faults like the Altyn Tagh fault system. The present study lays the foundation for Cowgill et al. (2004) by exploring the relationship between the topography and bedrock structure of the bend. In particular, we address three questions. (1) What is the spatial distribution of anomalous topography within

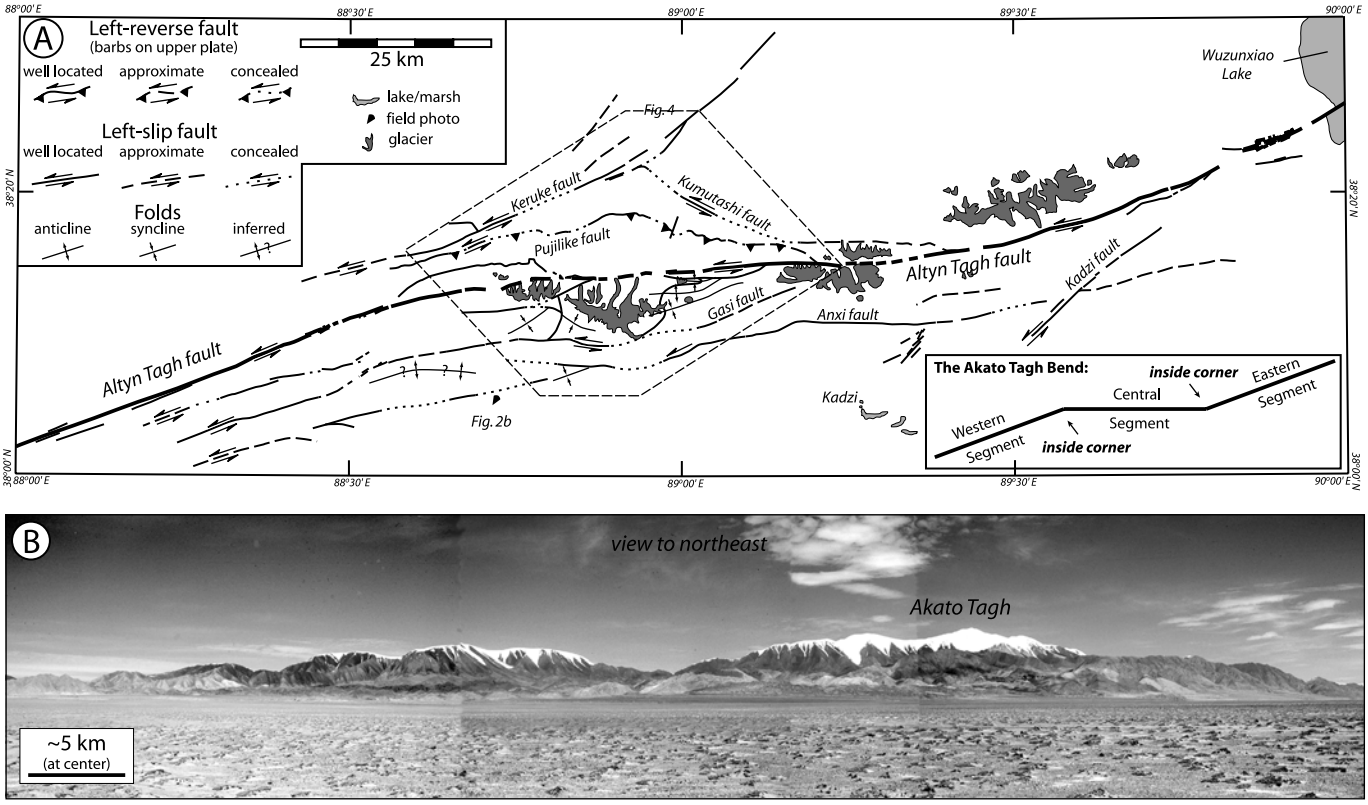

Figure 2. Overviews of the Akato Tagh restraining double bend. (A) Structural map of the Akato Tagh restraining bend compiled from our 1:100,000 structural mapping (Fig. 4) and analysis of CORONA imagery in addition to the active fault map of the Altyn Tagh fault (Chinese State Bureau of Seismology, 1992). Deformation of the strike-slip borderlands within the bend is partitioned into fault-perpendicular folding and fault-parallel strike-slip faulting. Inset shows locations of western, central, and eastern segments of the Akato Tagh bend and the positions of the two inside corners in the southwest and northeast sectors of the uplift. Polygon outlines Figure 4. (B) Photo-mosaic of peaks in the southwest inside corner, view to northeast. The Altyn Tagh fault is located behind the snow-capped peaks. Note that elevations increase from west to east, corresponding to areas that lie outside of, and within, the Akato Tagh restraining bend, respectively. Photo location as in part A.

the bend? (2) What structures produced this topography, and in particular, are the areas that flank the double bend cut by thrusts, similar to many other restraining bends? (3) What do the patterns of uplift and deformation tell us about the structural and topographic evolution of both this bend in particular, and restraining double bends in general?

The ~90-km-long Akato double bend (Figs. 1B and 2A) comprises three geometric segments (Fig. 2A, inset): a western section that strikes 070°, a central segment that strikes 087° between 88°37′E and 89°27′E longitude, and an eastern segment that strikes 067°. Where the segments join they create "inside corners" in the southwestern and northeastern sectors of the uplift (Fig. 2A, inset). Our investigation of the Akato Tagh range indicates that the bend is characterized by pronounced topographic and structural asymmetry and suggests that both the anomalous topography and fault-perpendicular shortening are concentrated within the two inside corners of the double bend. As we demonstrate, an important implication of such asymmetry is that the principal fault trace should undergo counterclockwise, vertical axis rotation during progressive deformation, thereby decreasing the bend angle and allowing the fault trace to smooth over time. This process may be important in helping to produce the decrease in fault-trace complexity with increasing total displacement that has been observed elsewhere (Wesnousky, 1988). Although restraining double bends are commonly flanked by thrusts, we observe that strike-slip faulting dominates within the Akato Tagh bend and that fault-perpendicular shortening has been absorbed by east-west trending folds. To explain the different styles of faulting within double bends, we postulate that the growth of topographic uplifts may alter the state of stress within some double bends and thereby favor strike-slip faulting adjacent to the bend.

In the following, we briefly review previous work on the topography and structures within restraining bends and then summarize the structural context of the central Altyn Tagh fault and the Akato Tagh uplift. We then examine the topography of the bend. This topographic analysis is followed by an analysis of the bedrock deformation within the western half of the double bend that is based on our 1:100,000 structural mapping and analysis of fault-zone fabrics. In subsequent sections we integrate our analyses of the topography and bedrock structure to infer the pattern of deformation within the bend. We conclude by exploring the kinematics and mechanics of restraining double bends.

BACKGROUND

Restraining Bend Topography and Structure

Previous work has highlighted the important relationship between shortening within active strike-slip restraining bends and the generation of local zones of anomalously high topography. For example, the geomorphology of the Santa Cruz Mountains has been shown to result from

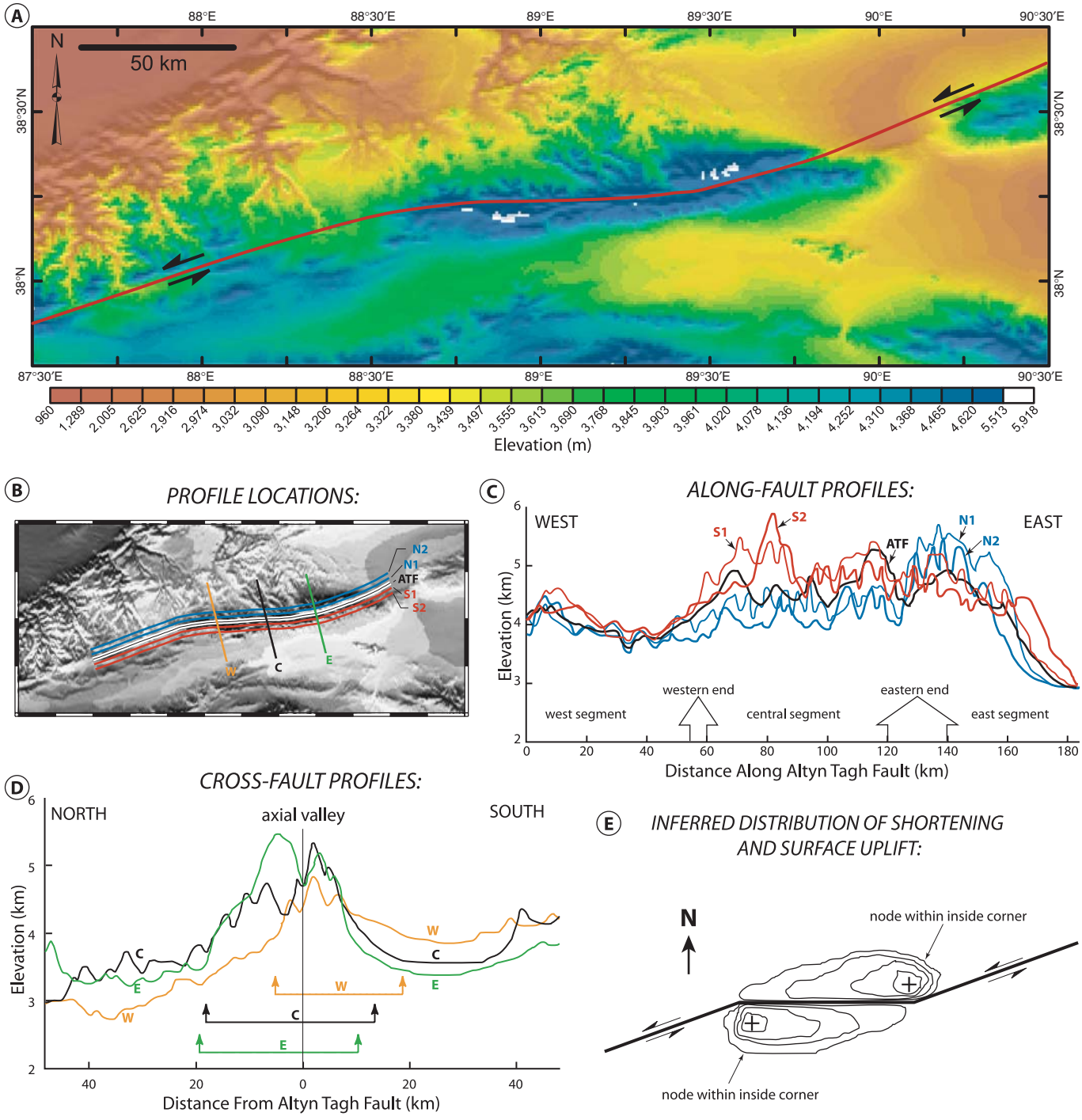

Figure 3. Akato Tagh topography. (A) Shaded-relief image generated from 1 km pixel resolution GTOPO-30 data set (http://edcdaac.usgs.gov/dataproducts.html). Elevations over 5500 m are white. Red line is the active trace of the Altyn Tagh fault. (B) Locations of topographic profiles sampled north (blue, N1-N2), south (red, S1-S2), and along (black, ATF) the Altyn Tagh fault. The locations of cross-fault profiles west (W), central (C), and east (E) are also shown. Base image from GTOPO-30 DEM. (C) Along-fault profiles sampled 3 and 6 km from the active trace. Black line is topography along the active trace. Topography is tallest in the two inside corners. (D) Cross-fault profiles. See B for the locations of these profiles. Arrowed brackets span the total width of the uplift and indicate that the topography is widest in the two inside corners. Topographic profiles were generated from GTOPO-30 using GMT software (Wessel and Smith, 1991). (E) Schematic diagram of the distribution of topography within the Akato Tagh bend.

the combined effects of tectonic uplift due to shortening across a bend in the San Andreas fault and decay of the elevated regions by erosion (Anderson, 1990, 1994). Bürgmann et al. (1994) found that regions of rapid unroofing in the Santa Cruz bend correspond with areas of high local relief and steep drainage slopes and concluded that thrusting along faults adjacent to the bend plays a primary role in producing the uplift. A region of both anomalous topography and elevated rock uplift rate also coincides with the San Bernardino bend along the southern San Andreas fault (Spotila et al., 1998; Spotila et al., 2001; Spotila and Sieh, 2000). Analog models of restraining double bends using sand (McClay and Bonora, 2001) and clay (Keller et al., 1997) demonstrated that bend angle and stepover width within the underlying basement fault together exert first-order control on the geometry of the bend uplift. However, it remains to be determined if regional double bends such as the Akato Tagh are indeed underlain by such basement faults that do not change geometry during progressive deformation. Elastic dislocation modeling has also been used to predict the distribution of uplifts within restraining double bends and stepovers (Bilham and King, 1989), and several comparisons between measured and modeled uplift patterns have been made (Bilham and King, 1989; Bürgmann et al., 1994; Kendrick et al., 2002). An important drawback of such dislocation models is that fault geometries are forced to remain static because most models do not explicitly account for finite strains, although attempts to address this problem have been made (e.g., Du and Aydin, 1995; Du and Aydin, 1993).

In contrast to the simplicity of elastic dislocation models, most natural double restraining bends are characterized by considerable structural complexity that likely reflects a similarly complex deformational history. Complex fault systems flank the Santa Cruz (Bürgmann et al., 1994) and San Bernardino (Spotila et al., 1998; Spotila et al., 2001; Spotila and Sieh, 2000) bends along the San Andreas fault, the Yammuneh double bend along the Dead Sea transform (Beydoun, 1999; Butler et al., 1997; Gomez et al., 2001 and references therein; Griffiths et al., 2000; Walley, 1998) and several double bends along the North Gobi-Altai (Bayasgalan et al., 1999; Cunningham et al., 1996; Cunningham et al., 1997; Owen et al., 1999) and Gobi-Tian Shan (Cunningham et al., 1997) strike-slip systems in southern Mongolia. Along some of these double bends, thrust and/or reverse faults flank the principal fault trace, whereas others are flanked by strike-slip faults and thus have a strikingly different structural style.

Structural Setting of the Central Altyn Tagh Fault

Early investigations of the Altyn Tagh fault based on Landsat image analysis and reconnaissance field work documented active, left-slip (Tapponnier and Molnar, 1977) and the recurrence of large-magnitude earthquakes (Molnar et al., 1987a; Molnar et al., 1987b). In contrast, recent studies have investigated the initiation age (Rumelhart, 1998; Yin et al., 2002), total offset (Cowgill et al., 2003; Ritts and Biffi, 2000; Yin and Harrison, 2000; Zheng, 1991, 1994), paleoseismic history (Chinese State Bureau of Seismology, 1992; Washburn et al., 2000; Washburn et al., 2001; Washburn et al., 2003), and both the Quaternary (Meriaux et al., 1997; Meriaux et al., 2000; Meriaux et al., 1998; Van der Woerd et al., 2001) and active slip rates (Bendick et al., 2000; Shen et al., 2001). Although the age of the active trace is debated, recent work indicates that the central segment of the system probably formed by ca. 49 Ma (Yin et al., 2002), whereas deformation along the eastern part of the system was under way by at least 30 Ma (Rumelhart, 1998; Yin and Harrison, 2000; Yue et al., 2001). The extent to which the central Altyn Tagh system accommodates significant strike-perpendicular shortening is also contested. Wittlinger et al. (1998) and Bendick et al. (2000) have both argued that Tibet-Tarim relative motion is transpressional, being partitioned onto northwest-directed thrusting along the North Altyn fault and pure strike-slip motion along the principal trace of the Altyn Tagh fault. Studies by Cowgill et al. (2000) and Shen et al. (2001) do not support significant fault-perpendicular motion along the North Altyn fault, suggesting the central Altyn Tagh fault system does not reflect regional transpression along the northwest margin of the Tibetan Plateau.

TOPOGRAPHY OF THE AKATO TAGH UPLIFT

The highest portions of the Akato Tagh range lie within the two inside corners of the bend, as the two zones of white pixels (areas over 5500 m elevation) in the DEM of Figure 3A highlight. To investigate the relationship between the geometry of the Altyn Tagh fault and the topography of the Akato Tagh bend in more detail, we constructed a series of topographic profiles across the restraining bend uplift (Figs. 3B–D). We assume that, to a first order, regions of anomalously high topography within a restraining bend will generally correspond with regions of high surface and/or rock uplift rate rather than being controlled by variations in rock type or climate. Geologic mapping described below indicates that rock types are generally similar within the bend, and previous work on bends similar in size to the Akato Tagh support such an assumption (e.g., Anderson, 1994; Bürgmann et al., 1994; Spotila et al., 1998; Spotila et al., 2001; Spotila and Sieh, 2000). We also assume that the structures absorbing fault-perpendicular shortening have generally uniform structural style so that horizontal motion is transformed into surface uplift in the same way throughout the bend.

Although the steep local relief of the Akato Tagh produces high amplitude, short wavelength variations along the topographic profiles in Figures 3C and 3D, their overall trends indicate that the topography is asymmetric both along and across strike. Fault-parallel profiles (Fig. 3C) north of the main fault trace gradually rise from west to east. Starting at a regional elevation of ~3900 m, the profiles begin to climb at the western end of the bend, ramping up to a maximum elevation of ~5500 m before steeply dropping to ~3000 m, ~40 km past the eastern end of the bend. In contrast, the profile along the Altyn Tagh fault is generally symmetric in that it rises steeply from an elevation of ~3800 m at the western end of the bend, plateaus at 4700 ± 500 m across the bend, and then drops steeply ~40 km past the east end of the bend to an elevation of ~3000 m. Fault-parallel profiles south of the active fault trace are skewed in the opposite sense as those to the north: they rise steeply and crest near the western end of the bend (Fig. 3C) and then gradually decline eastward.

Along-strike variations are also evident in the cross-fault profiles (Fig. 3D). In the western part of the bend, the uplift is narrower north of the fault than to the south, whereas near the eastern tip of the bend the opposite case holds. This set of profiles also indicates that on the north side of the bend the maximum width of the uplift is ~20 km and the regional elevation is ~3000–3500 m, whereas on the south side the maximum width is ~15 km and the regional elevation is ~3500–4000 m. The active trace does not coincide with the maximum elevation on any of these profiles, and instead lies within an axial valley.

In summary, the asymmetric topographic profiles indicate that the Akato Tagh consists of two topographic maxima, each of which lies within an inside corner of the bend (Fig. 3E). The contoured fields in Figure 3E schematically represent this distribution of topography. One node is located ~5 km south of the fault, at the western tip of the bend, and a second is ~5 km north of the fault, at the eastern end of the bend. Not only are the mountains highest at the two nodes, they are also widest normal to the fault in these areas. Along strike, the width and height of these maxima both decrease in the direction of block motion. What controls the

observed topographic asymmetry of the Akato Tagh restraining bend?

BEDROCK GEOLOGY OF THE AKATO TAGH AREA

To understand the topographic asymmetry and determine how transpressional deformation has been absorbed within the Akato Tagh, we mapped bedrock and active deformation at various scales throughout the bend (Fig. 2 and Cowgill et al., 2004). To investigate the bedrock deformation, we conducted 1:100,000 scale structural mapping in the western half of the bend in the Gasi area (Fig. 4). This region includes the southwest inside corner. We also measured fault-slip data and composite shear zone fabrics within brittle bedrock fault zones. To determine shear sense, we have used the criteria of Petit (1987) for brittle faults and the work of Cowan and Brandon (1994), Chester and Logan (1987), and Platt et al. (1988) for composite shear zone fabrics within gouge zones. Shear sense was also determined from the sense of rotation of asymmetric folds, where fold axes were found to lie within the plane of the fault at a high angle to the slip vector. For example, sinistral slip was inferred from steeply plunging folds with S asymmetry in down-plunge view and axes lying perpendicular to sub-horizontal fault striae. Brittle fault-slip data were also collected from small structures (microfaults) that were oriented parallel to the main fault either within the brittle shear zone or in rocks adjacent to the fault. Attitudes of planar features are reported as strike/dip using a right-handed, azimuthal convention. Thus, 070°/80° corresponds to a surface that strikes N70ºE and dips 80ºSE. Orientations of linear features such as slip vector azimuths are reported as trend/plunge with the trend in azimuthal format. We follow Twiss and Unruh (1998) and Gapais et al. (2000) in interpreting the brittle fault slip data in terms of kinematics rather than paleostress.

Altyn Tagh Fault

In the Gasi area (Fig. 4) the Altyn Tagh fault is expressed morphologically as an east-west trending axial valley that is typically ~1 km wide (Fig. 4, see also Cowgill et al., 2004). The valley is generally floored by Quaternary alluvium that conceals the underlying bedrock and is undeformed except in a narrow zone along the active trace. This trace typically lies near the southern edge of the axial valley and is generally defined by a series of discrete fault scarps having a component of south-side-up displacement (Fig. 4 and Cowgill et al., 2004). Cowgill et al. (2004) addresses the question of net transport direction along the Altyn Tagh fault. In contrast to the discrete active trace, deformation within the underlying bedrock fault zone is distributed over a zone that is 500–1000 m wide. Although bedrock exposures are generally limited to the margins of the axial valley, within these exposures rocks generally show penetrative brittle deformation including fault breccia and well-developed, composite shear zone fabrics.

Considering the breadth of the breccia zone and the potentially long history of activity during which fault zone fabrics may have rotated, it is not surprising that fault-slip data within the shear zone are scattered (Figs. 5A and 5B). Despite this scatter, both a mean fault surface oriented 080°/70° and a clustering of striae about a mean of 090°/25° are evident, indicating that strike-slip predominates on this reach of the Altyn Tagh fault in spite of its oblique orientation relative to the fault segments outside the Akato Tagh bend. Because slip sense was not determined for these striae, they reflect either dextral displacement with a small reverse component or sinistral displacement with a small extensional component. The latter is most likely considering the left-slip nature of the fault (e.g., Cowgill et al., 2004; Molnar et al., 1987a; Molnar et al., 1987b; Peltzer et al., 1989; Tapponnier and Molnar, 1977). Note that the mean fault surface strikes slightly more northward than the 085° to 090° strike of the Altyn Tagh fault zone in this area (Fig. 4).

Southern Strike-Slip Borderland

As Jamison (1991) first described, primary elements of a strike-slip system include the master fault and the associated strike-slip borderlands. In the case of the Akato Tagh bend, the master fault is the active trace of the Altyn Tagh fault and we define the strike-slip borderlands as the areas that lie within ~20 km on either side of this trace, because these regions coincide with the maximum width of the Akato Tagh range along the central segment of the bend (Figs. 2 and 3). Up to 15 km south of the main fault trace, this strike-slip borderland region is cut by a set of steeply dipping faults (Fig. 4) that parallel the main fault trace and bound structural panels that are characterized by upright folds. As indicated below, faults within this strike-slip borderland region are also predominantly left-slip, thus shortening across the western Akato Tagh appears to be absorbed primarily by these east-west trending folds.

Gasi Syncline

Between the Altyn Tagh and Gasi faults (Fig. 4), metavolcanic (mv) and low-grade metasedimentary basement (msed2) are non-conformably overlain by a sequence of lower Jurassic (Liu, 1988; Xinjiang Bureau of Geology and Mineral Resources, 1993) sandstone and conglomerate. Exposures at sites 802-3 and 801-3 (Fig. 4A) indicate that this contact is depositional. The Jurassic sequence is deformed by the Gasi syncline, a west-plunging, faulted fold (Fig. 4A). Geology around the Gasi and Anxi coal mines is structurally complex (Figs. 4B and 4C) and requires more detailed structural mapping to be fully understood. A northeast-striking fault with a sinuous map trace lies north of Xiong valley (Fig. 4; southeastern part of the map) and juxtaposes Jurassic conglomerate in the east against low-grade metasedimentary rocks (msed2) in the west. Shallowly raking striae at station 820-2 (Fig. 4) suggest strike-slip along this fault. Both this fault and the Jurassic strata up to 10 km east are folded by the Xiong anticline and syncline. Both folds have northeast-trending axial traces. The Xiong syncline may be a continuation of the Gasi syncline to the west (Fig. 4).

Gasi and Anxi Faults

The east-west striking and steeply north-dipping Gasi fault is defined by a ~200 m thick zone of breccia and cataclasite. Two populations of striae are on the mean fault surface (Fig. 5C). The dominant set plunges shallowly east and indicates left-slip. A less common set plunges steeply and indicates extension. Debris-flow breccias or glacial deposits of inferred Tertiary-Quaternary age (units QT?$_1$ and QT?$_2$) nonconformably overlie gneiss (gn3) south of the Gasi fault near the Gasi Coal Mine. The Tertiary-Quaternary (QT?) units are folded with upright axial surfaces (Fig. 4). These immature coarse-clastic deposits are unconsolidated and appear to be derived from both underlying basement units and Jurassic strata.

The Anxi fault system (Fig. 4) consists of a set of steeply dipping brittle faults that roughly coincides with the range front between the Gasi and Xiong valleys (Fig. 4). As the data in Figure 5D indicate, this fault is vertical (083°/89°) with gently raking striae that have a sinistral shear sense.

Northern Strike-slip Borderland

Keruke and Kumutashi Fault Zones

The active, left-slip Keruke fault (Fig. 4) crops out as a ~300 m wide zone of cataclasite and breccia. Within this shear zone, kilometer-long septae of marble evince both ductile and brittle deformation. A very similar structural style has been described from the Carboneras fault in Spain (Faulkner et al., 2003). Kinematic data compiled from throughout this zone

[1]Figure 4 is on a separate sheet accompanying this issue.

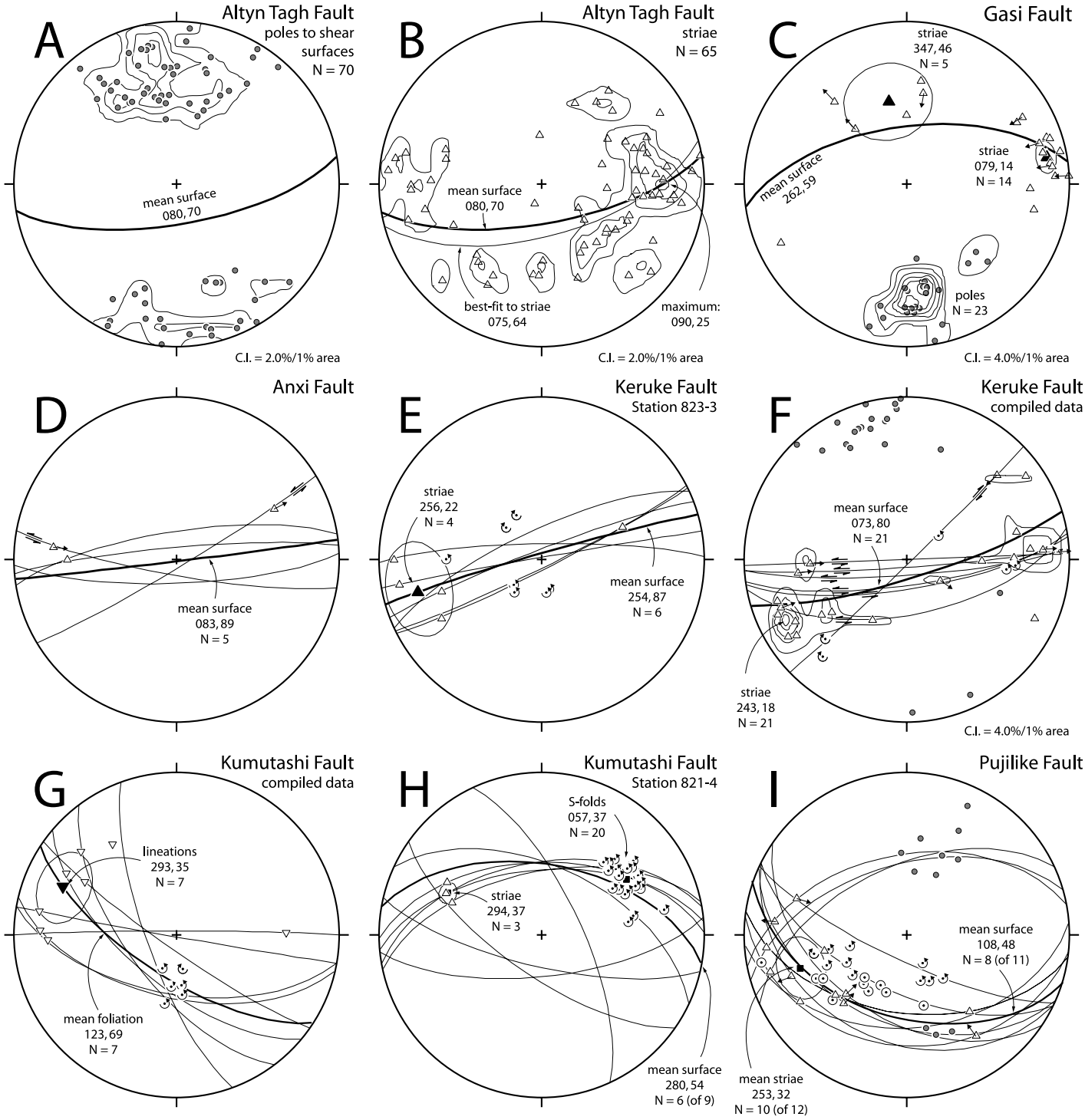

Figure 5. Equal-area, lower hemisphere stereograms of structural data from the main faults within Gasi map area. All faults are predominantly strike-slip except for the Pujilike fault, which is left-reverse slip. (A) poles to shear surfaces within the Altyn Tagh fault zone, (B) striae within the Altyn Tagh fault zone, (C) Gasi fault, (D) Anxi fault, (E–F) Keruke fault, (G–H) Kumutashi fault, (I) Pujilike fault. Averages of linear data (striae, fold axes, lineations) were found by calculating the mean vector or by finding the maxima of contoured data. Mean surfaces were determined by finding the mean vector to the poles of all surfaces. See text for discussion and Figure 4A for station locations.

(Fig. 5F) and from a single outcrop at station 823-3 (Fig. 5E) yield steeply dipping left-slip shear surfaces with striae and calcite-stretching lineations that plunge shallowly southwest. Total left separation along the Keruke fault is 23 ± 2 km, as indicated by the offset of the Kumutashi fault (Fig. 4). Kinematic data (Figs. 5G–5H) collected adjacent to the poorly exposed Kumutashi fault indicate that the slip vector is oriented 293°/35°. Sinistral motion is indicated by the rotation sense of steeply plunging, decimeter-scale, foliation-folding folds that lie within the Kumutashi fault zone (Fig. 5H).

Pujilike and North Makeqi Faults

The Pujilike fault coincides with a prominent break in slope in the western Kumutashi valley (Fig. 4), although the fault does not cut intermediate or young Quaternary deposits (Cowgill et al., 2004). The fault truncates compositional layering and foliation in the footwall and parallels compositional layering in the hanging wall. West of Pujilike valley, the Pujilike fault strikes northeast and has a straight map trace, indicating it dips steeply south (Fig. 4). This map pattern changes ~6 km west of the western Kumutashi valley, indicating that the eastern half of the Pujilike fault strikes northwest and dips moderately southwest. Coincident with this change in fault strike is an increase in deformation along the fault: in the eastern area, massive phosphatic dolomite marble is brecciated by abundant millimeter- to centimeter-scale gouge zones adjacent to the fault. The fault was mapped at the base of this deformation zone because the breccia blocks appear to be derived from the marble-slate (mb-sl) unit in the hanging wall. Southwest-dipping microfaults near the base of this breccia zone are typically oriented 108°/48°, with striae that cluster ~253°/32° (Fig. 5I). Left-reverse slip on the Pujilike fault is indicated by (1) the striae with sinistral slip indicators, (2) folds that trend at a high angle to the striae and record sinistral rotation, and (3) a hanging wall anticline at station 818-1 (Fig. 4). If this slip direction is representative of motion along the mapped trace of the Pujilike fault, then left-slip occurred along the western segment of the Pujilike fault.

The north Makeqi fault (Fig. 4) lies 2–4 km south of the Pujilike fault, west of the Pujilike valley. The map pattern of this fault indicates the fault surface dips more steeply at low elevations than where it crosses high topography, suggesting the fault has a concave-down geometry. In the valley wall at station 814-4, a pair of shallowly plunging folds suggests that this fault has a reverse component of displacement.

Shortening Estimates

Structural mapping of the bedrock deformation along the western half of the Akato Tagh restraining double bend suggests that deformation is more intense up to 15 km south of the Altyn Tagh fault than it is to the north. Specifically, the mapping indicates that in the Gasi area, the southern strike-slip borderlands are characterized by larger minimum shortening estimates, more intense faulting, narrower fault-bounded panels, and tighter folds than in the area north of the main trace (Fig. 4). There are several reasons to think that the strike-slip borderland structures formed along the central segment of the bend and thus reflect the same deformation field as the anomalous topography, rather than being inherited structures that have been transported into the bend region. Both existing maps (Chinese State Bureau of Seismology, 1992; Xinjiang Bureau of Geology and Mineral Resources, 1993) and our reconnaissance observations indicate that folds such as the Gasi syncline or the Xiong anticline are not present outside the bend region. In addition, active deformation along the western and eastern segments of the Akato Tagh bend is characterized by pure left-slip faulting (Cowgill et al., 2004) consistent with the idea that fault-normal shortening is restricted to the central part of the bend. Lastly, folding is the simplest mechanism for making the regions of high topography that is also consistent with the mapped structures.

In an attempt to evaluate the extent to which shortening differs between the northern and southern strike-slip borderlands, we have derived minimum shortening estimates for the Cenozoic, horizontal, north-south shortening within these two strike-slip borderland regions (Fig. 6). However, these estimates must be viewed with considerable skepticism, because the local stratigraphic thicknesses are poorly known and out-of-plane motion is likely to be quite large. These estimates are also conservative because we intentionally assumed structural geometries that minimized shortening wherever the reconstructed cross sections were poorly resolved. We emphasize that the aim of this analysis is simply to gain a qualitative sense of the amount of shortening within the bend. In no way do we mean to imply that we have truly determined total shortening.

We estimate that north-south shortening is at least 9 km on the south side of the Altyn Tagh fault (Fig. 6). This minimum is almost certainly too low because we have not accounted for north-south shortening in the structurally complex region between the Gasi syncline and the Gasi fault (Figs. 4A and 4C). This estimate assumes that all faults in the southern strike-slip borderland are pure left-slip structures, consistent with the fault-slip data for the Gasi and Anxi faults (Figs. 5C–5D). If this is an erroneous assumption, then our shortening estimate is too low. It also assumes that all folding reflects regional north-south shortening across the bend with no component of wrench folding. We think that this is the simplest assumption, considering that the folds are located within a transpressional restraining double bend where shortening perpendicular to the master fault is to be expected. If wrench folding is significant, then our minimum estimate is too high (e.g., Jamison, 1991; Krantz, 1995; Teyssier and Tikoff, 1998). Along section B–B′ we have assumed chevron fold geometries, consistent with the style of deformation observed in the field. Each fault-bounded panel was restored separately along this section. In section C–C′, the geometry of the Gasi syncline was estimated using the down-plunge view exposed in the map and by projecting the fold axis from near station 802-1 (Fig. 4A) into the plane of section. The unconformity between the Jurassic sedimentary rocks and the underlying metavolcanic basement has been extrapolated over an inferred anticline in the north half of section C–C′. We assume this fold exists due to the presence of the Xiong anticline ~10 km to the east (Fig. 4A), and that it has a form similar to the Gasi syncline.

Minimum north-south shortening is ~7 km on the north side of the Altyn Tagh fault, although it should be noted that this estimate is based on a poorly determined reconstruction of section D–D′ (Fig. 6). To derive this minimum estimate, we have only accounted for north-south shortening due to displacement along the Pujilike fault. We ignore Cenozoic shortening within the gneiss (gn1) complex and along the Keruke and Kumutashi faults because we found no major brittle faults within the gneiss (Fig. 4) and because the faults are left-slip structures (Figs. 5E–5H). We assume that the Pujilike fault is Cenozoic and related to deformation along the Altyn Tagh fault because it is brittle, strikes subparallel to the Altyn Tagh fault (Fig. 4), has equal components of dip-slip and strike-slip (Fig. 5I), and coincides with a prominent break in slope that may indicate it is still active. Estimation of slip along section D–D′ is difficult because we were not able to identify an offset marker common to both the mb-sl and marble+phyllite (mb-ph) units, or to establish the original relationship between them, although they are similar in terms of composition and metamorphic grade. However, the minimum offset along the Pujilike fault can be estimated by making two assumptions: (1) that the mb-ph unit overlies the mb-sl sequence, consistent with the reverse component of slip along the fault indicated by the fault-slip

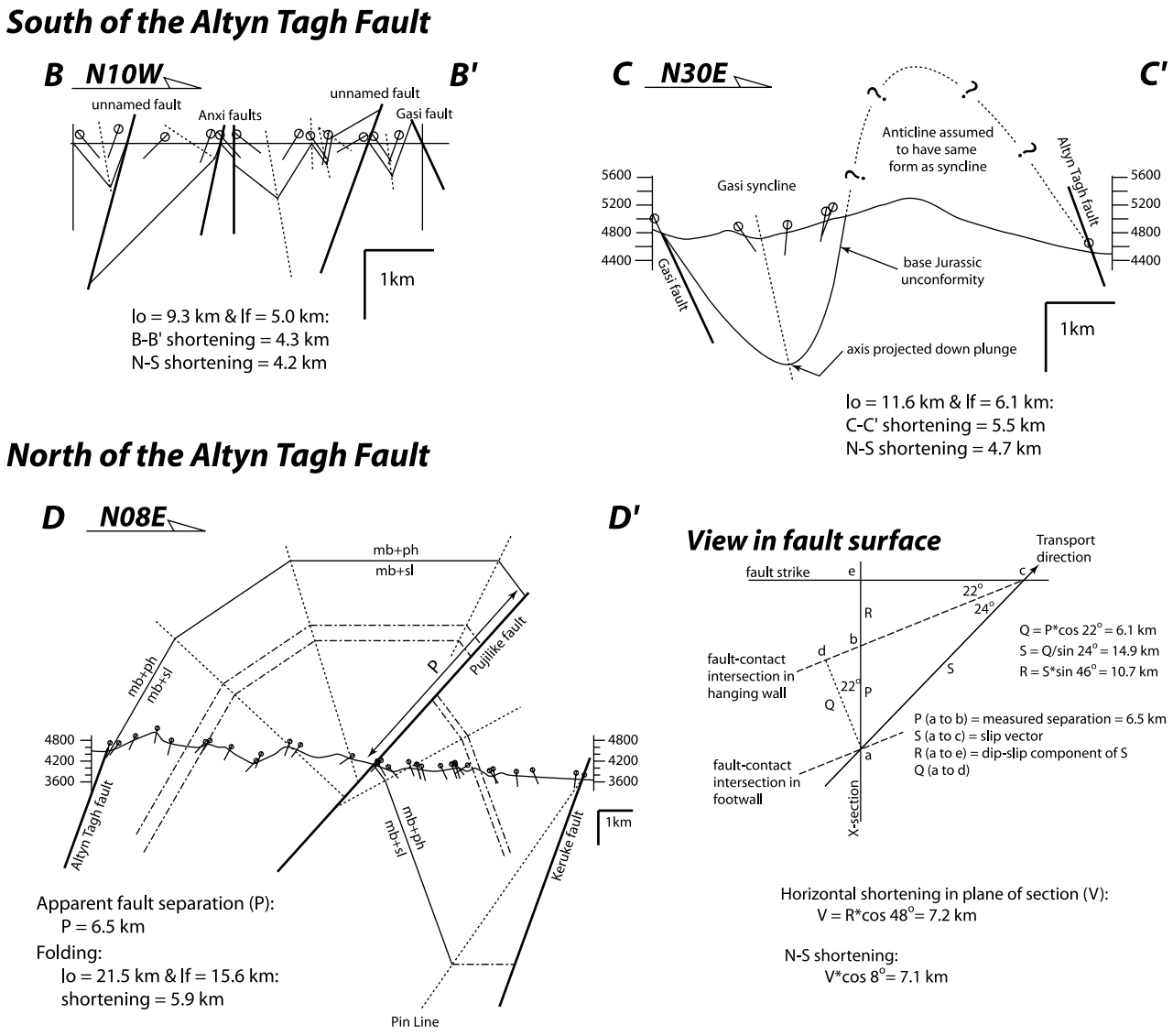

Figure 6. Cross sections used to derive minimum north-south shortening estimates. See Figure 4A for section locations and text for discussion of assumptions and calculations. Note that section D–D′ is not at the same scale as B–B′ or C–C′. North-south shortening values (S_{NS}) were calculated from shortening determined along the line of section (S_S) using $S_{NS} = S_S$ *cos η, where η is the angular difference between the trend of the section and true north. Shortening was determined by comparing original section line length (l_o) with final deformed length (l_f). North of the fault (section D–D′), ~7 km of north-south horizontal shortening was estimated by restoring oblique motion along the Pujilike fault. This shortening was determined as follows, using "view in fault surface" sketch (drawn looking down on the fault surface along the fault pole). Fault-slip data (Fig. 5I) indicate that the fault plane and transport vector are oriented 108°/48° and 253°/32°, respectively. Transport vector (line a–c) thus rakes 46°W. Line of intersection between the fault and contact between mb-sl and mb-ph is oriented 273°/17°, derived from intersection between fault and footwall layering (266°/69°). Intersection line rakes 22°W in the fault plane. Minimum separation (P) of the contact is 6.5 km, based on assumptions described in the text and on the inferred fold geometry. Only 4.4 km of north-south shortening would be required if this separation were produced by pure dip-slip along the Pujilike fault. However, the minimum dip-slip component should be 10.7 km to account for the out-of-plane, corresponding to a minimum of 7.2 km of 008°-directed horizontal shortening along the 48° dipping fault, or 7.1 km of north-south horizontal shortening. To simplify the geometry, we have made the section perpendicular to the fault in the sketch (true angle is 100°).

data (Fig. 5I), and (2) that the mb-sl and mb-ph units lie on the opposite limbs of an antiform, as suggested by their opposing dip directions and the hanging wall antiform near station 818-1 (Fig. 4A). The reconstruction of section D–D′ described in Figure 6 gives a minimum of ~7 km of north-south horizontal shortening.

Restoration of inferred folding along section D–D′ would yield an additional 6 km of 008-directed shortening. This shortening is not included in the minimum estimate due to the likelihood that the folding predates Cenozoic slip along the Altyn Tagh fault. Specifically, penetrative, isoclinal folding and transposed layering within the mb-ph unit reflects a phase of ductile deformation that predates the brittle Kumutashi, Keruke, and Pujilike faults. Although the age of this ductile deformation is undetermined, it may coincide with pre-Cenozoic ductile deformation that has been inferred elsewhere along the Altyn Tagh fault (e.g., Delville et al., 2001; Sobel et al., 2001). In addition, the mb-ph and mb-sl units may correlate with an isoclinally folded passive-margin unit north of Suekli (unpublished mapping by A. Yin and G. Gehrels) that also appears to have been folded prior to the onset of the Indo-Asian collision in the early Cenozoic.

Figure 7. Simplified maps illustrating structures around other restraining double bends. (A) Santa Cruz-Gabilan bend. First panel: location of Santa Cruz bend at northwestern end of a restraining double bend in the San Andreas fault; southeastern end is located near Pinnacles National Monument ("Pinnacles") (map simplified from Jennings, 1977). Box outlines location of structural map. Second panel: simplified structural map of Santa Cruz bend (modified from Bürgmann et al., 1994, and references therein); thrusts predominate. Third panel in each: shaded relief image generated from 30 m resolution SRTM elevation data (ftp://edcsgs9.cr.usgs.gov/pub/data/srtm/). Note concentrations of anomalously high topography in inside corners of the Santa Cruz-Gabilan restraining double bend (i.e., southern Santa Cruz Mountains and Gabilan Range). (B) San Bernardino bend. First panel: location of San Bernardino bend along southern San Andreas fault (simplified from Jennings, 1977). Box outlines structural map. Second panel: simplified structural map (modified from Spotila et al., 1998, and references therein); both strike-slip and thrust faults accommodate deformation adjacent to San Bernardino bend. (C) Yammuneh bend. First panel: location of Yammuneh restraining double bend at intersection of Dead Sea fault and Palmyrides thrust belt (modified from Ron et al., 1990). Box outlines structural map. Second panel: strike-slip faults and folds predominate adjacent to the Yammuneh bend (modified from Ron et al., 1990).

INTERPRETED PATTERN OF DEFORMATION

Two main interpretations can be drawn from our investigation of the bedrock structure within the strike-slip borderlands along the central segment of the Akato Tagh restraining double bend. First, fault-perpendicular shortening along this segment of the bend appears to be asymmetric along strike. This asymmetric pattern of deformation appears to characterize double bends along other large strike-slip faults. Second, transpression in the strike-slip borderlands appears to be partitioned onto left-slip faults and upright folds that trend east-west, parallel to the central segment of the Altyn Tagh fault. The predominance of strike-slip faulting within the strike-slip borderlands of the Akato Tagh contrasts with restraining bends where shortening is accommodated by thrusting.

Concentrated Shortening within the Inside Corners

Taken together, the topographic analysis and shortening estimates described above suggest that fault-perpendicular shortening along the central segment of the Altyn Tagh fault is highest within the two inside corners of the bend. In particular, structural mapping indicates that fault-perpendicular shortening along the central segment is more intense up to 15 km south of the main trace than it is to the north (Fig. 4). Comparison of this structural mapping with the topographic analysis (Fig. 3) indicates that this region of elevated shortening coincides with the node of high topography within the southwestern inside corner, suggesting that fault-normal folding was important in forming this area of high topography.

Figure 3 further indicates that the pattern of topography in the eastern half of the Akato Tagh uplift is the reverse of that in the west: the uplift is higher and wider north of the main trace than it is to the south. It is presently unclear how shortening is absorbed in the eastern half of the bend because this area has not been mapped in detail. The northern range front may be fault-bounded because it is morphologically sharp. However, this front is clearly overlapped by undeformed alluvial fans (Cowgill et al., 2004), indicating that this suspected fault is either no longer active or it moves at a slow rate. Active shortening within the northeastern sector of the Akato Tagh may also be absorbed by fault-parallel folds, left-reverse faults within the high topography up to 10 km south of the range front, or along blind thrusts (Herquel et al., 1999; Molnar et al., 1987a; Molnar et al., 1987b; Wittlinger et al., 1998).

Although it remains unclear how shortening is accommodated at the east end of the Akato Tagh bend, the correlation between the region of intense deformation and the area of high topography at the western end of the bend suggests that the asymmetric concentration of anomalous topography within the northeastern corner of the Akato Tagh bend reflects a similarly asymmetric deformation field. Mapping reported in Cowgill et al. (2004) indicates that Quaternary units are also asymmetrically distributed throughout the Akato Tagh bend, supporting the idea that uplift rates are highest within the two inside corners.

Several restraining double bends along other major strike-slip faults appear to have asymmetric patterns of topography and deformation similar to the Akato Tagh. One example is the Santa Cruz-Gabilan double bend in the northern San Andreas fault (Fig. 7A). Although the inside corner in the Santa Cruz area had less co-seismic surface uplift in the 1989 Loma Prieta earthquake than regions outside of the bend (Lisowski et al., 1989), various indicators suggest that this pattern is the reverse of the long-term tectonic uplift (Bürgmann et al., 1994). Rocks within the inside corner yield Late Miocene to Pliocene apatite fission track ages whereas ages outside the corner are Late Cretaceous to Early Paleocene, indicating denudation rates within the corner are higher than outside the bend (Bürgmann et al., 1994). The highest elevations, steepest slopes, and largest local relief all occur within ~10 km of the fault, directly northeast of the bend and within the inside corner (Bürgmann et al., 1994). The Gabilan Range defines a second topographic node at the south end of the bend (Fig. 7A), although it remains to be determined if this topographic high coincides with a region of elevated fault-perpendicular shortening and rock uplift. The Nemegt Uul bend along the Gobi-Tian Shan fault system (Owen et al., 1999) is also characterized by concentration of high topography within the inside corners of the bend. A right step in this east-west striking, left-lateral system forms inside corners in the northwestern and southeastern sectors of the uplift. The highest elevations and steepest relief within the Nemegt Uul are located within the southeastern inside corner (Owen et al., 1999).

Mechanical models predict that shortening should be focused into the two inside corners

Ⓐ ***Thrust-Dominated***

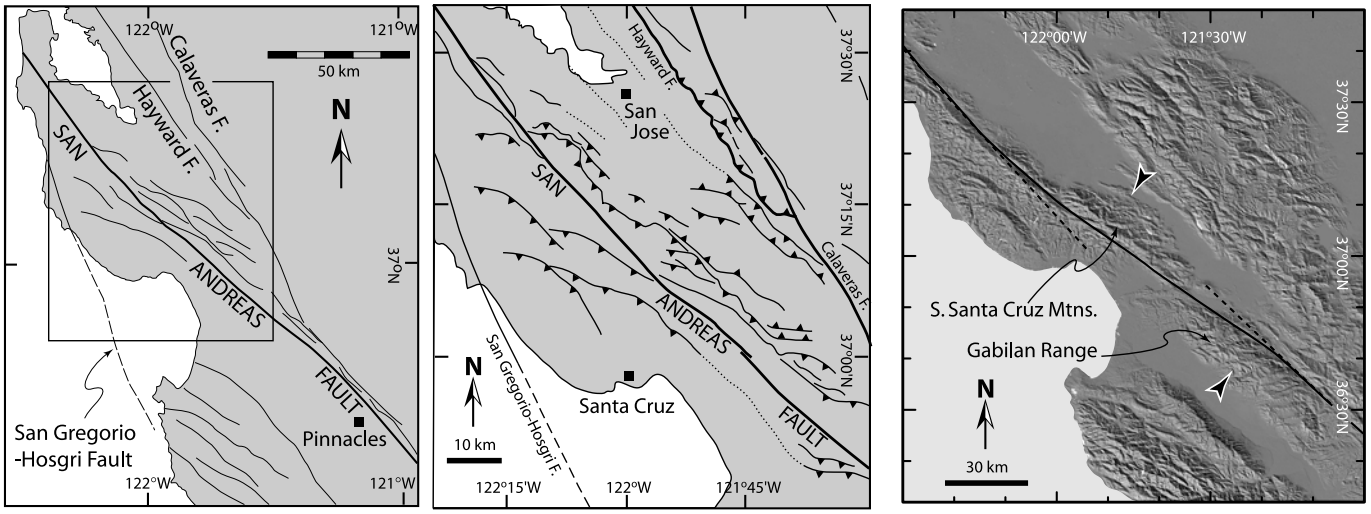

Ⓑ ***Mixed-Mode***

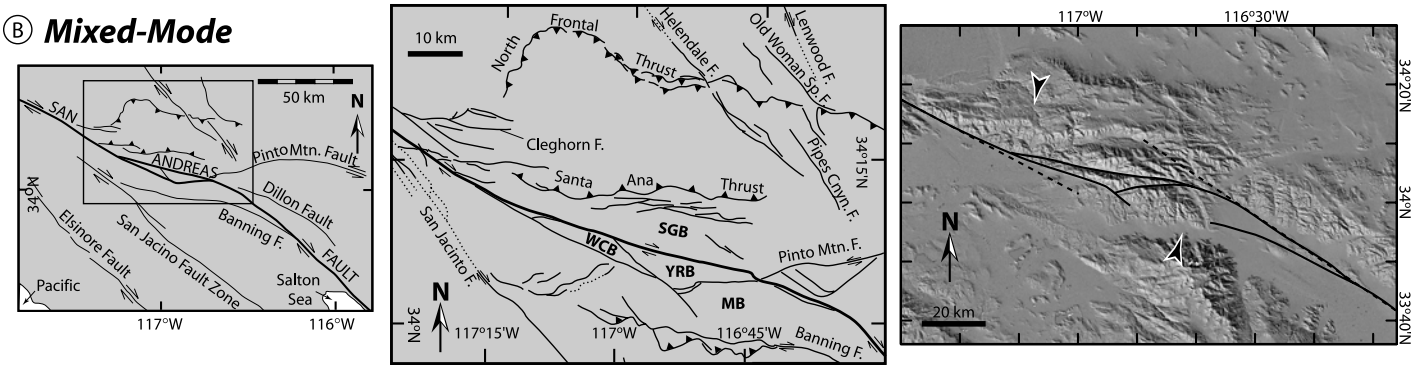

Ⓒ ***Strike-Slip Dominated***

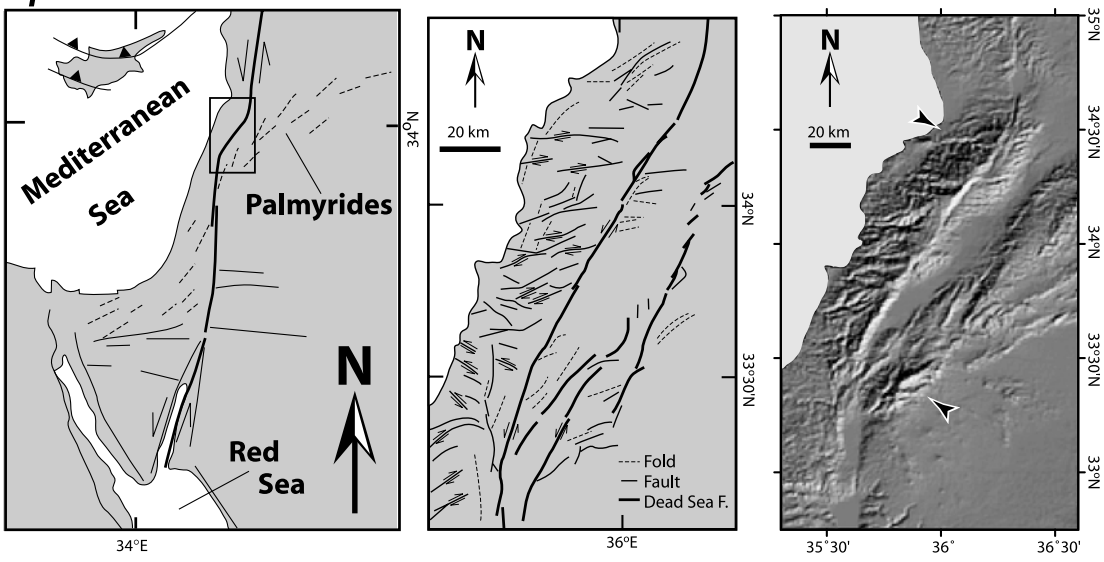

of a restraining double bend. For example, Bird (1999) used a thin-plate model to calculate the continuum strain rate in the vicinity of a right step along a left-slip fault. Strain rate contours are notably asymmetric around the modeled step with the highest rates occurring within the inside corners of the bend in a pattern similar to that shown by the topography around the Akato Tagh (e.g., compare our Fig. 3E with Fig. 5 of Bird, 1999). Bilham and King (1989) used boundary element methods to compute the spatial distribution of strain around geometric complexities along strike slip faults. Inasmuch as these linearly elastic models serve as first-order approximations to nonlinear crustal deformation, they indicate that when the bend angle is low, dilatational strains can be concentrated at the tips of the

double bend, rather than in the center (e.g., see Fig. 4 of Bilham and King, 1989).

Partitioned Deformation in the Strike-Slip Borderlands

The mapping and fault-slip data presented above indicate that transpressional deformation is partitioned within the strike-slip borderlands adjacent to the Akato Tagh restraining bend. In particular, bend-parallel displacement is accommodated by strike-slip faulting along a set of high angle faults that dips toward the main fault trace whereas bend-perpendicular shortening is absorbed by folding of the panels that lie between these strike-slip faults. Although the gross fault geometry is similar to that seen in other restraining bends (e.g., Sylvester, 1988; Woodcock and Fischer, 1986), the Akato Tagh bend is unusual in that its strike-slip borderland deformation is dominated by strike-slip faulting, rather than thrusting. To distinguish restraining double bends (such as the Akato Tagh) that are flanked by strike-slip faults from those that are flanked by thrusts, we refer to the former as "strike-slip dominated" and the latter as "thrust-dominated" bends. Below we speculate on the mechanics of these different types of bends.

Classic examples of thrust-dominated bends exist along the San Andreas fault in California, including the Santa Cruz bend (Fig. 7A) (Anderson, 1990, 1994; Bürgmann et al., 1994) and Wheeler Ridge along the Big Bend (Medwedeff, 1989, 1992). Additional examples from other strike-slip faults include the Montejunto bend along the Cercal fault in Portugal (Curtis, 1999) and a bend along the North Owl Creek transfer fault system in Wyoming (Paylor and Yin, 1993).

Although Woodcock and Fisher (1986) presented a number of examples of strike-slip dominated bends, the Yammuneh bend (Fig. 7C) along the Dead Sea Transform appears to be a particularly good example of this style of deformation. Like the Akato Tagh, the strike-slip borderlands flanking the Yammuneh bend are deformed by folds and strike-slip faults (Fig. 7C) (Beydoun, 1999; Butler et al., 1997; Gomez et al., 2001 and references therein; Griffiths et al., 2000; Walley, 1998). Major strike-slip fault strands within the bend include the Yammuneh, Serghaya, Ghab, and Roum faults. This system has been interpreted as a braided strike-slip system (Walley, 1988). The Yammuneh bend differs from the Akato Tagh bend in that conjugate strike-slip faulting is better developed whereas folding is less pronounced than along the Akato Tagh (e.g., compare Fig. 7C with Fig. 4).

Although the Santa Cruz and Akato Tagh bends serve as end-member examples of thrust- and strike-slip-dominated bends, respectively, there appears to be a spectrum of bend styles with some bends showing intermediate deformational modes. For example, transpressional deformation within the San Gorgonio bend along the San Andreas fault (Fig. 7B) is accommodated both by thrusting along the Santa Ana and North Frontal Thrust systems and strike-slip slivering/vertical extrusion of the Wilson Creek and Yucaipa blocks (Fig. 7B) (Spotila et al., 1998; Spotila et al., 2001; Spotila and Sieh, 2000). This "mixed-mode" of deformation also appears to characterize several restraining bends in Mongolia, including the Chandiman Uul (Cunningham et al., 1996) and Artsa Bogd bends (Cunningham et al., 1997) along the sinistral North Gobi Altai fault system, as well as the Nemegt Uul bend along the sinistral Gobi–Tian Shan fault system (Cunningham et al., 1996; Owen et al., 1999). In the Mongolian cases, the restraining-bend uplift is flanked by moderately to steeply dipping faults that root beneath the range. The panels that lie between these fault strands are typically folded. Although these strike-slip borderland faults were described primarily as thrusts, reported fault-slip data (Cunningham et al., 1996; Cunningham et al., 1997) indicate that strike-slip motion predominates along a number of these structures.

DISCUSSION

The pattern of deformation within the Akato Tagh double bend as interpreted from our structural mapping and topographic analysis has three main implications. First, focusing of bend-perpendicular shortening into the two inside corners of a double bend can cause the central fault segment to undergo vertical-axis rotation, thereby reducing the bend angle and smoothing the fault trace with progressive deformation (Fig. 8). Second, the observed deformation field can be used to estimate the age of the bend (Fig. 9). Third, changes in fault strength or variations in the state of stress due to an evolving topographic load may be important in controlling the mechanics of faulting around restraining double bends and may explain why some bends are thrust-dominated whereas others are flanked by strike-slip faults (Figs. 10–12). In the sections that follow we discuss each of these hypotheses in more detail.

Bend Rotation

If the regions adjacent to the fault behave as two purely rigid blocks, shortening and surface uplift within the double bend should be uniform along strike and the bend angle should remain essentially constant during progressive deformation (Fig. 9A). If bend-perpendicular shortening is concentrated into the two inside corners of a restraining double bend, however, then the principal fault should undergo vertical-axis rotation during progressive deformation if it continues to occupy the same surface within the bend (Fig. 8A). Subsidiary fault strands adjacent to a bend, such as the Pujilike and Anxi faults in the case of the Akato Tagh bend (Figs. 2 and 4), create fault-bounded slivers that can be thought of as either subsidiary blocks or part of a strain-softened zone that borders the principal fault. In this case, the total, far-field shortening across the bend can be uniform along strike, but the deformable zones can allow along-strike variations in where that shortening is absorbed. As a result, the principal fault trace can undergo vertical-axis rotation. In the case of the Akato Tagh bend, we infer that shortening within the deformable zone is largest in the southwestern and northeastern sectors of the uplift. Such along-strike asymmetry in shortening should cause the western end of the central segment of the Altyn Tagh fault to move south relative to the eastern end, producing a counterclockwise rotation of the trace of the Altyn Tagh fault during progressive deformation (Fig. 8A). This counterclockwise rotation is consistent with that expected inside a zone of sinistral shear.

Counterclockwise, vertical-axis rotation of fault-bounded blocks within sinistral restraining double bends has been demonstrated in analog experiments (Keller et al., 1997; McClay and Bonora, 2001). Likewise, rotation of the principal fault trace appears to have occurred within the Yammuneh bend in the Dead Sea transform (Fig. 7C). Paleomagnetic data indicate that rocks within the southwestern inside corner of the bend have undergone 69° ± 13° of counterclockwise, vertical-axis rotation (Ron, 1987; Ron et al., 1984). Ron et al. (1990) argued that these rotations were produced by domino-style slip on multiple sets of dextral strike-slip faults that accommodated distributed strike-slip shear of the strike-slip borderland region, in which case the principal fault does not rotate over time. Westaway (1995) provided a kinematic model involving bend rotation to explain these data. An alternative idea is that the vertical-axis rotation results from the concentration of bend-perpendicular shortening into the two inside corners of the bend (e.g., Fig. 8A).

Vertical-axis rotation of a restraining bend via along-strike variations in the strain field will lengthen the principal fault trace as deformation progresses, assuming that the bend width (the fault-perpendicular distance between the two straight segments outside the bend) does not

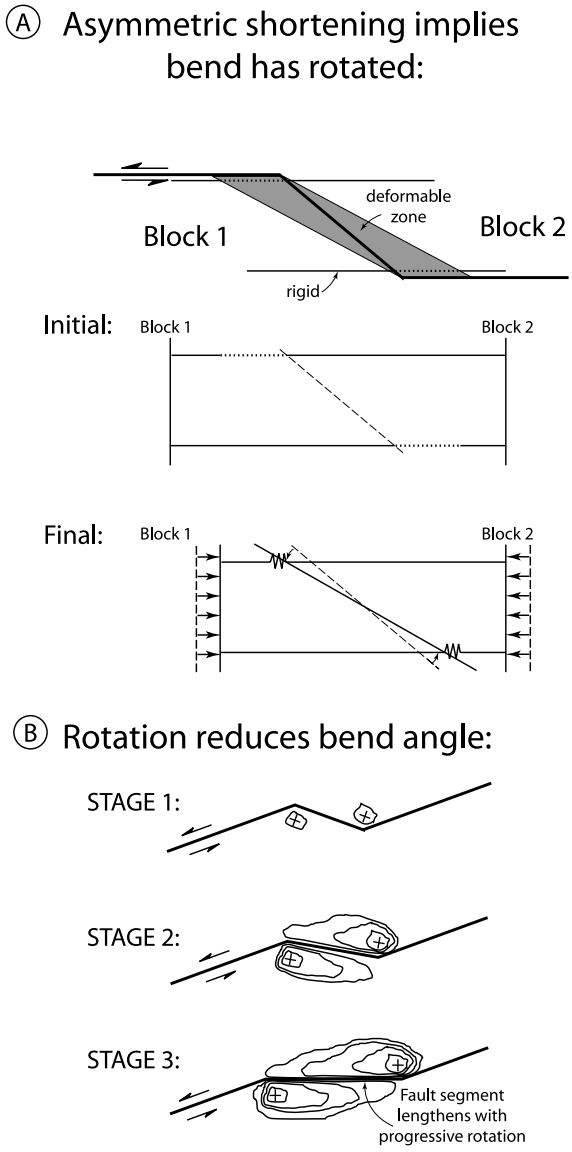

Figure 8. The along-strike asymmetry of deformation adjacent to the Akato Tagh bend suggests that the principal fault has experienced counterclockwise, vertical-axis rotation over time. (A) Plan-view sketch illustrating how across-strike variations in distribution of shortening can cause the fault to rotate. Note that total shortening between blocks 1 and 2 is uniform along the whole length of the bend. (B) Rotation of the bend will reduce bend angle, allowing such geometric complexities to smooth or heal as slip accumulates. Contours represent schematically topography generated by bend-perpendicular shortening. See text for additional discussion.

change. Strike-slip faulting in the strike-slip borderlands may help to accommodate this fault-parallel extension as the bend rotates to progressively lower angles. Zachariasen and Sieh (1995) illustrated this process for the releasing stepover between the Homestead Valley and Emerson Faults in the Mojave Desert of southern California (e.g., see their Fig. 10).

Vertical-axis rotation of a restraining double bend will cause it to smooth as deformation progresses, because both the bend angle and the degree of transpression across it will decrease as the bend rotates. Thus, the two-node mode of deformation facilitates progressive flattening of a restraining double bend in a process similar to footwall collapse of a ramp within a thrust system. As a result, restraining double bends in which fault-perpendicular shortening is concentrated within the two inside corners will gradually smooth themselves with progressive deformation. Wesnousky (1988) showed that the number of fault steps per unit length of fault decreases as a function of total offset along the strike-slip fault. The process of bend smoothing by vertical-axis rotation during progressive deformation described here is one potential mechanism to produce such observed reduction in fault-zone complexity during progressive deformation. Washburn et al. (2003) calculated a steps/length value of 0.006 for a 700 km long reach of the Altyn Tagh fault between ~86°E and 92°E, similar to values for the Garlock (0.004) and Whittier-Elsinore (0.009) faults, which have total offsets of 64 km and 10–40 km, respectively. The high steps/length value for the Altyn Tagh fault supports the idea that both the Akato Tagh bend and the active trace of the Altyn Tagh fault are young (below and Cowgill et al., 2004) and have not accumulated the full 475 ± 70 km of total displacement along the Altyn Tagh system determined by Cowgill et al. (2003).

How Old is the Bend?

The section on concentrated shortening within the inside corners (above) proposes an interpretation in which the asymmetric topography and our structural mapping of the Akato Tagh are taken together to indicate that shortening is asymmetrically distributed within the restraining double bend. Further work is needed to test this model, particularly structural mapping of the eastern half of the bend. To accommodate this uncertainty, each of the following four independent age estimates emphasizes a different aspect of the geometry and structural style of the bend: whereas some of these perspectives are consistent with our hypothesis regarding the deformation field, others presume alternative patterns of deformation. We adopt this approach so as to evaluate the range in bend ages implied by reasonable models for its evolution.

Estimate #1: Mass Balance

The first calculation is a simple mass-balance estimate. Specifically, it combines an estimate of the amount of excess crust within the uplift with a simple model relating slip on the straight sections to flux of crust into the bend (Figs. 9A and B). The cross-fault topographic profiles (Fig. 3D) indicate that the regional elevation outside the Akato Tagh is ~3500 m. We calculate ~3100 km^3 of rock lies above this elevation in the vicinity of the Akato Tagh. To obtain a maximum age, we maximize the volume of thickened crust by assuming that it is locally compensated via Airy isostasy (Fig. 9B). In this case the volume of the root (V_r) needed to support the topographic volume (V_t) is given by $V_r = V_t[\rho_c/(\rho_m - \rho_c)]$ (Turcotte and Schubert, 1982)

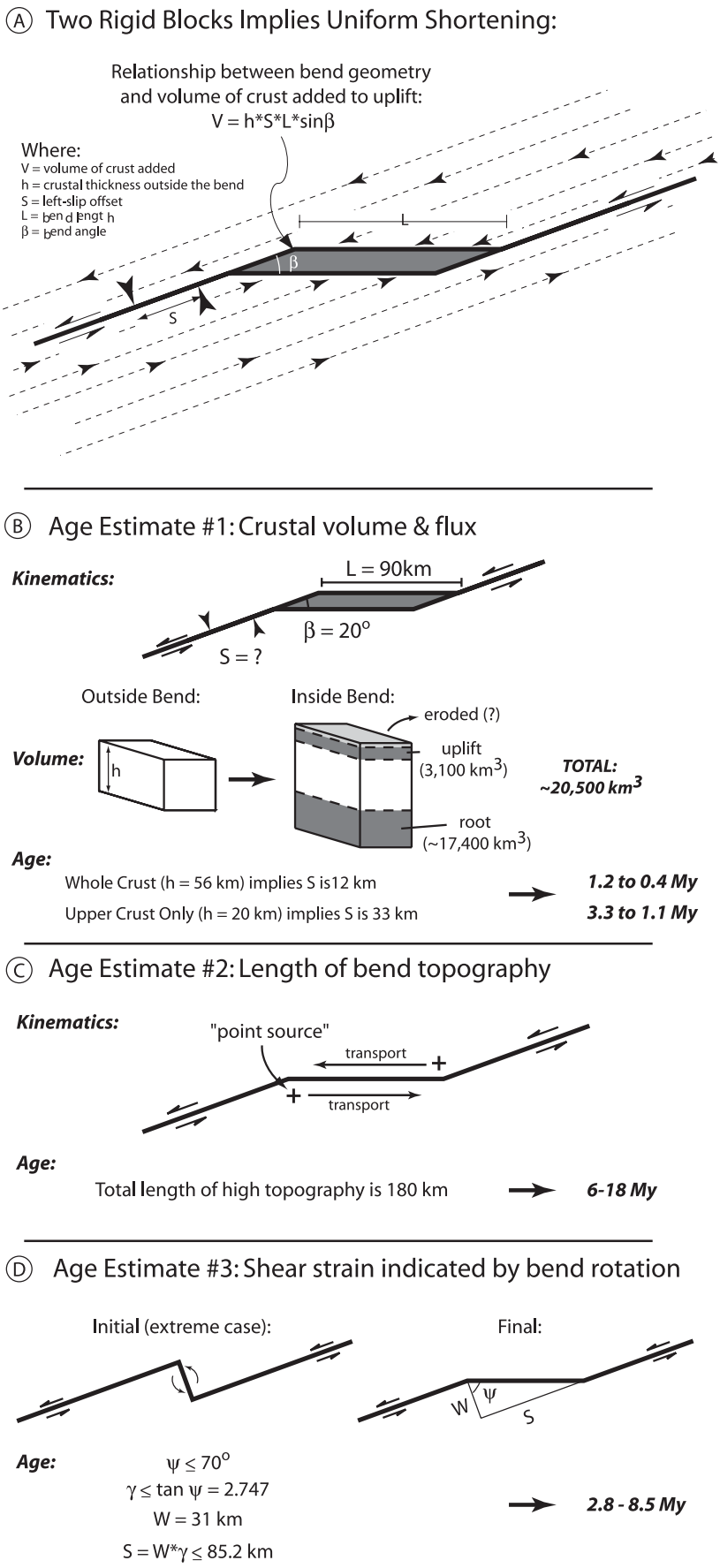

Figure 9. Sketches illustrating bend age estimates. (A) Rigid blocks. If the crust adjacent to the fault deforms as rigid blocks, then shortening and uplift should be uniformly distributed along strike. This is not evident in the geology, geomorphology, or topography of the Akato Tagh. Sketch also shows the relationship between fault geometry and the volume of crust brought into the bend by slip of amount S along the Altyn Tagh fault. This excess volume of crust will be stored in the bend as thickened crust, or it will leave the bend via erosion, subduction, lower crustal flow, or transport along the fault. (B) The first estimate of the age of the Akato Tagh bend is based on estimated volume of excess crust presently contained within the bend and the simple model illustrated in (A) that relates slip on the straight segments outside of the bend to the flux of crust into the stepover region. Assuming a reasonable range of slip rates (10–30 mm/y) and crustal thicknesses (20–56 km) indicates that the bend is only a few million years old. (C) The second estimate for the age of the bend is based on the along-strike extent of anomalous topography within the restraining bend uplift, and is based on an assumption that the uplift occurs only within the two inside corners of the bend. Anomalous topography extends ~90 km past each inside corner in the direction of block motion. At slip rates of 30–10 mm/y it would take 6–18 m.y. to generate such a length of elevated topography. (D) The third age estimate is based on the maximum likely vertical-axis rotation and the width of the shear zone. At reasonable slip rates (30–10 mm/y) it would take only 3–9 m.y. to produce this shearing. See text for additional discussion of age estimates.

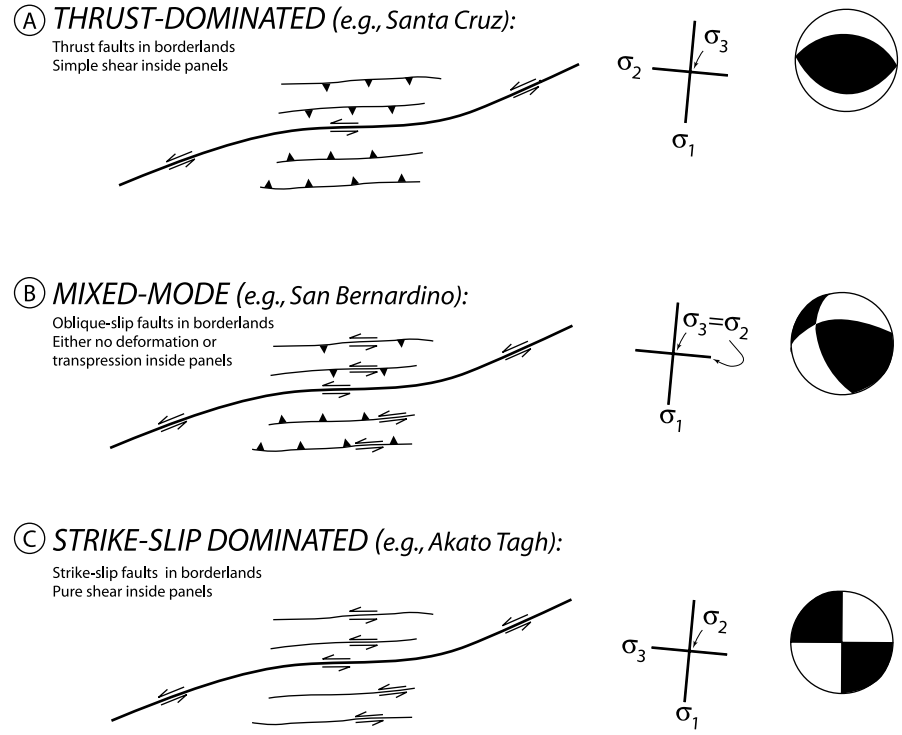

Figure 10. Sketches illustrating how the state of stress within the strike-slip borderlands might control the style of faulting adjacent to a restraining double bend. (A) Thrust-dominated bends, with $\sigma_v = \sigma_3$, (B) mixed-mode bends, with $\sigma_v = \sigma_h = \sigma_2 = \sigma_3$, (C) strike-slip bends, in which $\sigma_v = \sigma_2$.

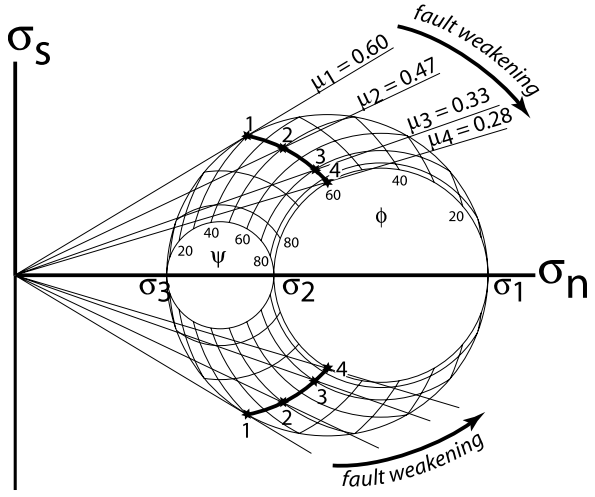

Figure 11. 3-D Mohr circle showing how the state of stress might evolve within the strike-slip borderlands of a restraining double bend if the strength of the strike-slip borderland faults decreases during progressive deformation. Points 1–4 indicate different stress states corresponding to progressively decreasing fault strength. In this example, the angle between the fault and σ_1 is fixed (i.e., φ is held constant). Thus, when the fault first forms (Point 1), σ_3 is vertical and σ_2 is horizontal (i.e., $\omega = 90°$). As μ decreases, ω will decrease and ψ will increase so that in the final state (Point 4) σ_2 is vertical and σ_3 is horizontal (i.e., $\psi = 90°$). See text for additional assumptions and discussion.

where ρ_c and ρ_m are crustal and mantle densities, respectively. If ρ_c = 2800 kg m^{-3}, ρ_m = 3300 kg m^{-3}, and V_f = 3100 km^3, then V_r = 17400 km^3, giving 20500 km^3 as a maximum for the volume of excess crust presently contained within the double bend. As Figure 9A demonstrates, for a double bend of length L and angle β, slip of amount S outside the double bend introduces volume $V = h\,S\,L\,\sin\beta$ of crust into the double bend, where h is the thickness of the crust outside the double bend. Using V = 20500 km^3, L = 90 km, $\beta = 20°$, and h = 56 km (Ma, 1980) indicates S is 12 km. At slip rates of 10–30 mm/y the double bend is only 1.2–0.4 million years old. If only the upper crust thickens within the bend (i.e., h = 20 km) then S = 33.3 km and the double bend is 3.3–1.1 million years old. These values overestimate the age of the bend if the range is flexurally supported, because flexural support of the topography reduces the volume of excess crust that is stored within the root. They underestimate the age of the bend if mass has been removed, for example by erosion. Large magnitudes of denudation in the mapped area are unlikely, because rocks north of the fault comprise low grade slate and marble whereas those to the south are unmetamorphosed Jurassic sedimentary rocks that unconformably overlie crystalline basement rocks.

Estimate #2: Topographic Advection

Anderson (1990, 1994) explored both the generation of topography and its decay due to geomorphic attack as crust is advected through a restraining bend along a strike-slip fault. That analysis inspires a second estimate for the age of the bend that is derived from considering the fault-parallel extent of the uplifted topography (Fig. 9C). For this estimate, we assume that the topography is generated only in the two inside corners and is then transported passively along the fault. In this case, the fault-parallel extent of elevated topography provides an estimate for the magnitude of slip since the double bend formed. Because the topography decays as it is transported (e.g., Anderson, 1994), this estimate is a minimum. Although this model is not consistent with our preferred interpretation for how the bend formed, we consider it so as to entertain a competing model for bend evolution. Both north and south of the fault, elevated topography extends for ~90 km west and east, respectively, of the inside corners, suggesting a total of 180 km of left slip. It would take between 6 and 18 million years to accumulate this amount of offset at rates of 30–10 mm/y.

Estimate #3: Bend Rotation

The third method uses the inferred vertical-axis rotation of the bend and its present

geometry to calculate an age based on estimates of the magnitude of the shear strain (Fig. 9D). For this calculation, we assume that the stepover spacing (W) between the western and eastern fault segments remained constant, because we see no structural evidence of large-magnitude fault-perpendicular shortening or extension along the western and eastern segments of the Akato Tagh bend (e.g., Cowgill et al., 2004) such as would be expected if the stepover width had changed. We also adopt an extreme initial bend geometry in which the central fault segment starts perpendicular to the western and eastern fault sections (Fig. 9D). This assumption is very likely wrong. For example, experiments by McClay and Bonora (2001) demonstrated that the morphology of restraining bend uplifts is sensitive to initial fault geometry, and comparison between the model uplifts and the Akato Tagh suggests that 90° is too large. On the other hand, it is unclear if the models of McClay and Bonora (2001) accurately represent large bends like the Akato Tagh because these simulations fail to account for erosion, pore-fluid effects, or the thermal and flexural effects of faulting, and they also adopt a simple geometry in which an initially undeformed and homogenous Navier-Coulomb material overlies a localized "basement" fault. In the end, we assume an initial 90° bend because this will maximize the amount of rotation and thereby provide an upper bound for the bend age. Rotation from a 90° to 20° bend angle over a 31 km wide zone corresponds to a shear strain (γ) of 2.747 (Fig. 9D) and a total slip of ~85 km. It would take no more than 8.5 m.y. to accumulate this amount of rotation at slip rates of 30–10 mm/y.

Estimate #4: Shortening

A final age estimate can be derived using the minimum amounts of shortening discussed above. Figure 6 indicates that the minimum north-south shortening at the western end of the bend is 16 km, although this could be as high as 22 km if the folding north of the Altyn Tagh fault is included. These north-south shortening values correspond to minimum strike-slip offsets of 47 and 64 km, respectively, along the western and eastern segments of the bend, assuming that the geometry of the bend remains constant and that motion outside the bend is parallel to the ~070-striking fault sections. At slip rates of 30–10 mm/y, the bend would only need to exist for 1.6–4.7 m.y. to accumulate 47 km of offset or for 2.1–6.4 m.y. if the minimum offset is 64 km. These age estimates are minimum values, like the offset estimates upon which they are based.

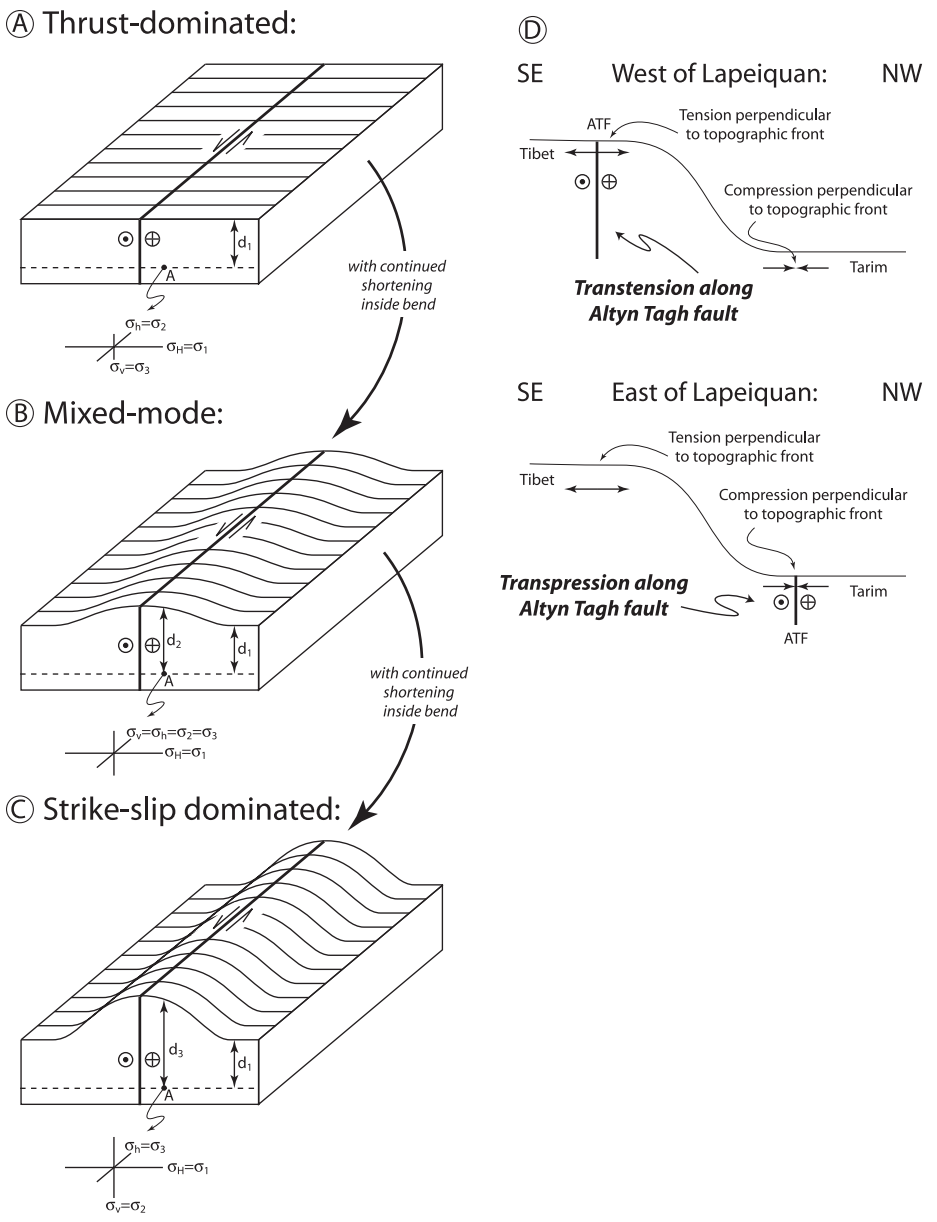

Figure 12. Sketches illustrating how the state of stress adjacent to a restraining double bend might change during growth of restraining-bend topography. (A) Thrust-dominated bend; initially bend topography is low, such that $\sigma_v = \sigma_3$ and $\sigma_h = \sigma_2$. (B) Growth of topography by thrusting might increase vertical stress until $\sigma_v = \sigma_h = \sigma_2 = \sigma_3$, producing a mixed-mode bend. (C) Continued bend-perpendicular shortening and thickening might cause σ_v to exceed σ_h, resulting in $\sigma_v = \sigma_2$ and a strike-slip dominated bend. (D) Sketches illustrating how the observed style of faulting along the Altyn Tagh fault varies as a function of the position of the fault trace relative to the margin of the Tibetan Plateau. Such variation suggests that topographic stresses constitute a significant fraction of the regional stresses and thus supports the hypothesis that the style of faulting within the Akato Tagh bend may be influenced by the topographic stresses that result from the restraining bend uplift.

Bend Age Versus Age of Altyn Tagh System

Of the four independent estimates, two give upper bounds on the age of the Akato Tagh bend. Importantly, both estimates appear to be too low for this structure to be as old as the Altyn Tagh fault system as a whole. This discrepancy either indicates that our age estimates are erroneous or that the double bend formed after the Altyn Tagh fault system developed. Addressing the discrepancy in the age of the Akato Tagh and the

Altyn Tagh system is a main theme of Cowgill et al. (2004) because it is unlikely that the age estimates are so far in error that the bend and the system can be the same age. For example, if the double bend has existed since the Altyn Tagh system first formed at ca. 49 Ma (Yin et al., 2002), then it should contain more than an order of magnitude more excess crust than we estimate is within the double bend. Although we have tried to maximize the volume of excess crust within the double bend, and thus its age, our estimate is simplified in that it does not account for crust lost from the uplift via erosion, subduction of part of the crustal root, or lower crustal flow (e.g., Avouac and Burov, 1996; Bird, 1991; McKenzie et al., 2000; Royden, 1996). It seems unlikely that a significant volume of crust has been lost via erosion, because the preservation of unmetamorphosed Jurassic rocks within the topographic maxima in the Gasi area indicates exhumation is limited to less than 5 km: based on reported stratal thicknesses near the western edge of the Qaidam basin (Lee, 1984; Métivier et al., 1998, and references therein), no more that 3.5–4.5 km of Cenozoic deposits appears to have capped the Jurassic rocks prior to their unroofing within the Akato Tagh bend.

Strike-slip versus Thrust-Dominated Restraining Bends

Why are the Akato Tagh strike-slip borderlands cut by strike-slip faults instead of thrusts, and why are some restraining double bends thrust-dominated whereas others are flanked by strike-slip faults? We speculate that local perturbations in the state of stress in the immediate vicinity of a restraining double bend determine the extent to which thrust- or strike-slip faults predominate in the adjacent strike-slip borderlands (Fig. 10). According to classical faulting theory (e.g., Anderson, 1951), the principal stress axes around a strike-slip faults should be oriented such that $\sigma_1 = \sigma_H$, $\sigma_2 = \sigma_v$, $\sigma_3 = \sigma_h$, where $\sigma_1 > \sigma_2 > \sigma_3$ are the principal stresses, σ_v is the vertical stress, and σ_H and σ_h are the maximum and minimum horizontal stresses, respectively. We suggest that thrust-dominated bends reflect a local state of stress that is $\sigma_H = \sigma_1$, $\sigma_h = \sigma_2$, $\sigma_v = \sigma_3$ (Fig. 10A), whereas strike-slip dominated bends develop when $\sigma_H = \sigma_1$, $\sigma_h = \sigma_3$, and $\sigma_v = \sigma_2$ (Fig. 10C). Mixed-mode bends might reflect $\sigma_H = \sigma_1$, $\sigma_h = \sigma_v = \sigma_2 = \sigma_3$ (Fig. 10B) so that both strike-slip and thrusting can occur within the strike-slip borderlands.

There are several reasons to expect departures from classical faulting theory inside a bend. Both analytical and numerical models indicate that changes in the strike of a strike-slip fault are likely to cause the state of stress within geometric complexities to deviate from that in the far field (e.g., Chester and Chester, 2000; Chester and Fletcher, 1997; Saucier et al., 1992; Segall and Pollard, 1980). In addition, the state of stress adjacent to major faults appears to be strongly controlled by fault strength (e.g., Ben-Avraham and Zoback, 1992; Bunds, 2001; Mount and Suppe, 1987; Zoback et al., 1987), although the extent to which faults are weak has been questioned (Scholz, 2000; Scholz and Saucier, 1993). Borehole breakouts, earthquake focal mechanisms and fold orientations along the San Andreas fault all indicate that σ_1 trends roughly perpendicular to the fault, in turn suggesting that the fault is too weak to support the shear stresses expected from the oblique orientation of σ_1 in the far field (e.g., Mount and Suppe, 1987; Townend and Zoback, 2000; Zoback et al., 1987). The presence of thrusts and thrust-cored folds in the San Andreas strike-slip borderlands further suggests that $\sigma_v = \sigma_3$ adjacent to the fault (Mount and Suppe, 1987).

We suggest that two processes may be important in controlling the differences in the state of stress and thus structural style seen within restraining bends: (1) progressive changes in the effective strength of faults in the strike-slip borderlands (Fig. 11), or (2) progressive changes in the state of stress within the strike-slip borderlands resulting from the growth of restraining bend topography (Fig. 12). The basic elements of these two speculations are outlined below, although a complete mechanical analysis of these hypotheses is beyond the scope of the present study.

Evolving Fault Strength

One way to produce variations in the style of strike-slip borderland faults is to allow their strength to decrease as deformation progresses (Fig. 11), and Holdsworth et al. (2001) have recently reviewed mechanisms and examples by which such fault-zone weakening may occur. For the present analysis, assume that the angles between the pole to the fault surface and the σ_1, σ_2, and σ_3, axes are φ, ω, and ψ, respectively. These values are related by $(\cos \varphi)^2 + (\cos \psi)^2 + (\cos \omega)^2 = 1$ (Jaeger and Cook, 1969). We start with the assumption that σ_1 trends at a high angle to the fault and that $\sigma_H = \sigma_1$, $\sigma_h = \sigma_2$, $\sigma_v = \sigma_3$ inside the restraining double bend, such as might be the case along a bend in a weak fault. We further presume that the strike-slip borderlands are initially undeformed, that they follow Byerlee's law (i.e., $\mu = 0.60$), and that they fail according to classical faulting theory. In this case, the strike-slip borderland faults should initiate as thrusts that dip ~30° and strike subparallel to the central segment of the bend. Point 1 on Figure 11 shows the state of stress when the strike-slip borderland fault first forms and indicates that $\varphi = 60°$, $\omega = 90°$, $\psi = 30°$ in this initial stage.

Now consider the effect of decreasing fault strength (μ) while keeping both the magnitudes of σ_1, σ_2, and σ_3 and angle φ fixed (i.e., the fault does not rotate and the trend of σ_1 at a high angle to the main strike-slip fault is fixed by the weakness of the master fault). As Figure 11 indicates, weakening of the fault should cause the σ_2 and σ_3 principal stresses to rotate relative to the fault in the strike-slip borderland. For example, Point 2 on Figure 11 shows that when $\mu = 0.47$, $\psi = 50°$ and $\omega = 54.5°$, whereas Point 3 indicates that when $\mu = 0.33$, $\psi = 70°$ and $\omega = 37.3°$. Eventually σ_2 and σ_3 switch their orientations relative to the initial state represented by point 1: Point 4 on Figure 11 shows that when $\mu = 0.28$, $\psi = 90°$, and $\omega = 30°$. Thus, in the final state, $\sigma_H = \sigma_1$, $\sigma_h = \sigma_3$, and $\sigma_v = \sigma_2$.

Figure 11 suggests that progressive fault weakening might convert strike-slip borderland thrusts into strike-slip faults, thereby explaining the various styles of faulting seen adjacent to double restraining bends (e.g., Fig. 7). This model predicts that faults adjacent to thrust-dominated bends should be strong whereas faults flanking strike-slip dominated bends are weak. The model also predicts that the strike-slip borderland faults should dip gently. Thus, we do not favor this model for the Akato Tagh, because the strike-slip borderland faults dip steeply (Figs. 4 and 5).

Evolving State of Stress Due to Growing Topography

The importance of topography in affecting the state of stress within the lithosphere has been demonstrated by a number of studies (e.g., Fleitout and Froidevaux, 1982; Molnar and Lyon-Caen, 1988; Richardson and Coblentz, 1994), and includes work specifically on the topographic stresses associated with linear ridges and small slopes (Liu and Zoback, 1992; McTigue and Mei, 1981; Savage and Swolfs, 1986). Thus, a second possibility is that the topography along restraining double bends may perturb the local state of stress and thereby produce the different structural styles in Figure 7. According to this idea, bends with minimal topography are predicted to be thrust-dominated ($\sigma_H = \sigma_1$, $\sigma_h = \sigma_2$, and $\sigma_v = \sigma_3$), whereas bends containing large topographic uplifts are predicted to be strike-slip dominated ($\sigma_H = \sigma_1$, $\sigma_h = \sigma_3$, and $\sigma_v = \sigma_2$). An important implication of this idea is that the style of faulting within a restraining bend might change systematically as deformation progresses and the topographic relief within the bend grows.

In this second analysis we again assume that 1) the geometric complexity along the strike-slip

fault produces an initial state of stress within the bend that is $\sigma_H = \sigma_1$, $\sigma_h = \sigma_2$, $\sigma_v = \sigma_3$, 2) that σ_1 trends at a high angle to the main strike-slip fault, and 3) that the strike-slip borderlands fail according to classical faulting theory. We further assume that σ_h and σ_H are tectonically controlled and remain constant in magnitude while σ_v is lithostatic (i.e., $\sigma_v = \rho g h$, where ρ is rock density, g is gravitational acceleration, and h is depth).

To illustrate the effect of growing topography, consider how the state of stress changes at Point A that lies at an initial depth d_1 within the restraining double bend shown in Figure 12. When deformation first starts (Fig. 12A), the state of stress at point A is $\sigma_H = \sigma_1$, $\sigma_h = \sigma_2$, $\sigma_v = \sigma_3$ and the bend is thrust-dominated. As deformation progresses (Fig. 12B), the amount of bend-perpendicular shortening should increase (e.g., Fig. 8A), thereby causing the bend uplift to grow. As a result, the magnitude of σ_v at point A might increase until $\sigma_v = \sigma_h$ (Fig. 12B), thereby converting the bend from thrust-dominated to mixed-mode (Fig. 7C). With continued shortening and growth of the uplift (Fig. 12C), the magnitude of σ_v might eventually exceed σ_h, producing a state of stress at point A that is $\sigma_H = \sigma_1$, $\sigma_v = \sigma_2$, $\sigma_h = \sigma_3$ and thereby converting the bend from mixed-mode into strike-slip dominated.

Several observations support our postulate that topographic stresses may be important in controlling the style of faulting along the Altyn Tagh fault, particularly around the Akato Tagh bend. Structural mapping of the western half of the bend (Fig. 4) indicates that strike-slip faults are present where the bend uplift is highest ~5 km south of the Altyn Tagh fault, but that oblique slip occurs up to ~8 km north of the main fault, where the topography is lower. In addition, the style of faulting along the main trace of the Altyn Tagh fault appears to depend on whether or not the fault lies at the crest or the base of the topographic step that defines the northwest margin of the Tibetan Plateau (Fig. 12D). The fault crosses this ~2000 m high topographic front between 91°E and 93°E, near Lapeiquan (Fig. 1). The Altyn Tagh fault lies near the crest of the mountain front and has a small component of fault-perpendicular extension ~50–130 km west of Lapeiquan (Peltzer et al., 1989; Washburn et al., 2003; Washburn et al., 2001). In contrast, 10 km west of Subei (Fig. 1), the fault lies at the base of the topographic margin and has a component of fault-perpendicular shortening (Meyer et al., 1998). As Figure 12D indicates, these along-strike differences in the style of faulting are consistent with the idea that the style of deformation may be influenced by topographically induced variations in the state of stress along or adjacent to the Altyn Tagh fault, but these differences could also be due to subtle variations in fault geometry (i.e., a gentle releasing and restraining bends in the Xorkoli and Subei regions, respectively).

CONCLUSIONS

The following conclusions can be drawn from our investigation of bedrock deformation along the Akato Tagh restraining double bend.

1. Topographic profiles both along and across the Altyn Tagh fault indicate the Akato Tagh uplift is asymmetric. The highest and widest areas of the range are expressed as two topographic maxima located within the inside corners of the double bend.

2. Structural mapping of the Gasi area, along the western half of the Akato Tagh bend, indicates that transpressional deformation is partitioned into fault-parallel strike-slip motion along east-west striking left-slip faults and fault-perpendicular shortening along similarly oriented folds on the south side of the fault.

3. The node of high topography within the southwestern inside corner of the bend coincides with a region of apparently locally elevated strain. We conclude that the other topographic high in the northeastern inside corner is probably underlain by another region of strong fault-perpendicular shortening. In this case, the asymmetric distribution of topography should reflect a similar asymmetry in the distribution of fault-perpendicular shortening.

4. Concentration of fault-perpendicular shortening into the two inside corners of a left-lateral restraining double bend may cause the principal fault to undergo clockwise vertical-axis rotation with progressive deformation. Such rotation may cause the bend angle, and thus the degree of transpression across the bend, to decrease progressively, thereby smoothing the bend and allowing this geometric complexity to heal.

5. Using the kinematics of deformation around the Akato Tagh bend and previous determinations of slip rate along the Altyn Tagh fault, we derived four estimates for the age of the bend. These estimates indicate that the bend is most likely only a few m.y. old, and that it is no more than ~18 m.y. old. All four of these estimates indicate the double bend is considerably younger than the Altyn Tagh fault system. Thus, either the active trace is old and has only recently been deformed to form the double bend, or both the active trace and the double bend are young.

6. The predominance of strike-slip faulting in the strike-slip borderlands of the Akato Tagh bend differs from the thrusting that characterizes several other restraining double bends. To explain this difference, we suggest that local variations in the state of stress may control the style of faulting within the strike-slip borderlands adjacent to the bend. This hypothesis predicts that restraining bends may undergo an evolution from thrust-dominated to mixed-mode and eventually to strike-slip dominated deformation due to either the growth of topography or the weakening of strike-slip borderland faults during progressive deformation.

ACKNOWLEDGMENTS

Eric Cowgill benefited from discussions with Todd Ehlers, Paul Kapp, Jing Liu, Rowena Lohman, Nadine McQuarrie, Mike Murphy, Mike Taylor, and Zhengkang Shen. Jim Spotila, Arthur Sylvester, and Associate Editor Doug Walker provided very helpful reviews. We thank Elizabeth Catlos, Jian Anhua, the Tarim Petroleum Corporation, and the First Seismological Bureau for their assistance in the field. Kristen Ebert digitized the topographic contour lines in Figure 4. Stereoplots were generated using Stereonet v. 4.9.6 developed by Rick Allmendinger. This project was funded by NSF Continental Dynamics grant EAR9725599.

REFERENCES CITED

Anderson, E.M., 1951, The Dynamics of Faulting and Dyke Formation with Applications to Britain: Edinburgh, Oliver and Boyd, 206 p.

Anderson, R.S., 1990, Evolution of the northern Santa Cruz Mountains by advection of crust past a San Andreas fault bend: Science, v. 249, p. 397–401.

Anderson, R.S., 1994, Evolution of the Santa Cruz Mountains, California, through tectonic growth and geomorphic decay: Journal of Geophysical Research, v. 99, no. B10, p. 20,161–20,179, doi: 10.1029/94JB00713.

Avouac, J.P., and Burov, E.B., 1996, Erosion as a driving mechanism of intracontinental mountain growth: Journal of Geophysical Research, v. 101, no. B4, p. 17,747–17,769, doi: 10.1029/96JB01344.

Bayasgalan, A., Jackson, J., Ritz, J.-F., and Carretier, S., 1999, 'Forebergs,' flower structures, and the development of large intracontinental strike-slip faults: the Gurvan Bogd fault system in Mongolia: Journal of Structural Geology, v. 21, p. 1285–1302, doi: 10.1016/S0191-8141(99)00064-4.

Ben-Avraham, Z., and Zoback, M.D., 1992, Transform-normal extension and asymmetric basins: An alternative to pull-apart models: Geology, v. 20, p. 423–426, doi: 10.1130/0091-7613(1992)0202.3.CO;2.

Bendick, R., Bilham, R., Freymueller, J., Larson, K., and Yin, G., 2000, Geodetic evidence for a low slip rate in the Altyn Tagh fault system: Nature, v. 404, p. 69–72, doi: 10.1038/35003555.

Beydoun, Z.R., 1999, Evolution and development of the Levant (Dead Sea Rift) Transform System: a historical-chronological review of a structural controversy, *in* MacNiocaill, C., and Ryan, P.D., eds., Continental Tectonics: The Geological Society [London] Special Paper 164, p. 239–255.

Bilham, R., and King, G., 1989, The morphology of strike-slip faults: examples from the San Andreas fault, California: Journal of Geophysical Research, v. 94, no. B8, p. 10,204–10,216.

Bird, P., 1991, Lateral extrusion of lower crust from under high topography in the isostatic limit: Journal of Geophysical Research, v. 96, no. B6, p. 10,275–10,286.

Bird, P., 1999, Thin-plate and thin-shell finite-element programs for forward dynamic modeling of plate deformation and faulting: Computers and Geosciences, v. 25, p. 383–394, doi: 10.1016/S0098-3004(98)00142-3.

Bunds, M.P., 2001, Fault strength and transpressional tectonics along the Castle Mountain strike-slip fault, southern Alaska: Geological Society of America Bulletin, v. 113, p. 908–919, doi: 10.1130/0016-7606(2001)1132.0.CO;2.

Bürgmann, R., Arrowsmith, J.R., Dumitru, T., and McLaughlin, R., 1994, Rise and fall of the southern Santa Cruz Mountains, California, from fission tracks, geomorphology, and geodesy: Journal of Geophysical Research, v. 99, no. B10, p. 20,181–20,202, doi: 10.1029/94JB00131.

Butler, R.W.H., Spencer, S., and Griffiths, H.M., 1997, Transcurrent fault activity on the Dead Sea Transform in Lebanon and its implications for plate tectonics and seismic hazard: Journal of the Geological Society of London, v. 154, p. 757–760.

Chester, F.M., and Chester, J.S., 2000, Stress and deformation along wavy frictional faults: Journal of Geophysical Research-Solid Earth, v. 105, no. B10, p. 23,421–23,430, doi: 10.1029/2000JB900241.

Chester, F.M., and Logan, J.M., 1987, Composite planar fabric of gouge from the Punchbowl fault, California: Journal of Structural Geology, v. 9, no. 5/6, p. 621–634.

Chester, J.S., and Fletcher, R.C., 1997, Stress distribution and failure in anisotropic rock near a bend on a weak fault: Journal of Geophysical Research, v. 102, no. B1, p. 693–708, doi: 10.1029/96JB02791.

Chinese State Bureau of Seismology, 1992, The Altyn Tagh active fault system (in Chinese with English abstract): Beijing, China, Seismology Publishing House, 319 p.

Cowan, D.S., and Brandon, M.T., 1994, A symmetry-based method for kinematic analysis of large-slip brittle fault zones: American Journal of Science, v. 294, p. 257–306.

Cowgill, E., Yin, A., Wang, X.F., and Zhang, Q., 2000, Is the North Altyn fault part of a strike-slip duplex along the Altyn Tagh fault system?: Geology, v. 28, p. 255–258, doi: 10.1130/0091-7613(2000)0282.3.CO;2.

Cowgill, E., Yin, A., Harrison, T.M., and Xiao-Feng, W., 2003, Reconstruction of the Altyn Tagh fault based on U-Pb geochronology: Role of back thrusts, mantle sutures, and heterogeneous crustal strength in forming the Tibetan Plateau: Journal of Geophysical Research, v. 108, no. B7, 2346, doi: 10.1029/2002JB002080.

Cowgill, E., Arrowsmith, J.R., Yin, A., Wang, X.-F., and Chen, Z., 2004, The Akato Tagh bend along the Altyn Tagh fault, NW Tibet 2. Active deformation and the importance of transpression and strain hardening within the Altyn Tagh system: Geological Society of America Bulletin, v. 116, p. 1443–1464.

Crowell, J.C., 1974, Origins of late Cenozoic basins in southern California, *in* Dickinson, W.R., ed., Tectonics and Sedimentation: Tulsa, Oklahoma, Society of Economic Paleontologists and Mineralogists, Special Publication 22, p. 190–204.

Cunningham, W.D., Windley, B.F., Dorjnamjaa, D., Badamgarov, J., and Saandar, M., 1996, Late Cenozoic transpression in southwestern Mongolia and the Gobi Altai Tien Shan connection: Earth and Planetary Science Letters, v. 140, no. 1-4, p. 67–81, doi: 10.1016/0012-821X(96)00048-9.

Cunningham, W.D., Windley, B.F., Owen, L.A., Barry, T., Dorjnamjaa, D., and Badamgarav, J., 1997, Geometry and style of partitioned deformation within a late Cenozoic transpressional zone in the eastern Gobi Altai Mountains, Mongolia: Tectonophysics, v. 277, no. 4, p. 285–306, doi: 10.1016/S0040-1951(97)00034-6.

Curtis, M.L., 1999, Structural and kinematic evolution of a Miocene to Recent sinistral restraining bend: the Montejunto massif, Portugal: Journal of Structural Geology, v. 21, p. 39–54, doi: 10.1016/S0191-8141(98)00095-9.

Delville, N., Arnaud, N., Montel, J.-M., Roger, F., Brunel, M., Tapponnier, P., and Sobel, E., 2001, Paleozoic to Cenozoic deformation along the Altyn Tagh fault in the Altun Shan massif area, eastern Qilian Shan, northeastern Tibet, China, *in* Hendrix, M.S., and Davis, G.A., eds., Paleozoic and Mesozoic Tectonic Evolution of Central and Eastern Asia: From Continental Assembly to Intracontinental Deformation: Boulder, Colorado, Geological Society of America Memoir 194, p. 269–292.

Du, Y.J., and Aydin, A., 1993, The maximum distortional strain-energy density criterion for shear fracture propagation with applications to the growth paths of en-echelon faults: Geophysical Research Letters, v. 20, no. 11, p. 1091–1094.

Du, Y.J., and Aydin, A., 1995, Shear fracture patterns and connectivity at geometric complexities along strike-slip faults: Journal of Geophysical Research, v. 100, no. B9, p. 18,093–18,102, doi: 10.1029/95JB01574.

Faulkner, D.R., Lewis, A.C., and Rutter, E.H., 2003, On the internal structure and mechanics of large strike-slip fault zones: Field observations of the Carboneras fault in southeastern Spain: Tectonophysics, v. 367, p. 235–251, doi: 10.1016/S0040-1951(03)00134-3.

Fleitout, L., and Froidevaux, C., 1982, Tectonics and topography for a lithosphere containing density heterogeneities: Tectonics, v. 1, no. 1, p. 21–56.

Gapais, D., Cobbold, P.R., Bourgeois, O., Rouby, D., and d Urreiztieta, M., 2000, Tectonic significance of fault-slip data: Journal of Structural Geology, v. 22, p. 881–888, doi: 10.1016/S0191-8141(00)00015-8.

Gomez, F., Meghraoui, M., Darkal, A.N., Sbeinati, R., Darawcheh, R., Tabet, C., Khawlie, M., Charabe, M., Khair, K., and Barazangi, M., 2001, Coseismic displacements along the Serghaya fault: an active branch of the Dead Sea Fault System in Syria and Lebanon: Journal of the Geological Society, v. 158, p. 405–408.

Griffiths, H.M., Clark, R.A., Thorp, K.M., and Spencer, S., 2000, Strain accommodation at the lateral margin of an active transpressive zone: Geological and seismological evidence from the Lebanese restraining bend: Journal of the Geological Society of London, v. 157, p. 289–302.

Herquel, G., Tapponnier, P., Wittlinger, G., Jiang, M., and Shi, D., 1999, Teleseismic shear wave splitting and lithospheric anisotropy beneath and across the Altyn Tagh fault: Geophysical Research Letters, v. 26, no. 21, p. 3225–3228, doi: 10.1029/1999GL005387.

Holdsworth, R.E., Strachan, R.A., Magloughlin, J.F., and Knipe, R.J., 2001, The Nature and Tectonic Significance of Fault Zone Weakening: Geological Society Special Publication 186, 328 p.

Jaeger, J.C., and Cook, N.G.W., 1969, Fundamentals of Rock Mechanics: London, Methuen and Co. Ltd., 513 p.

Jamison, W.R., 1991, Kinematics of compressional fold development in convergent wrench terranes: Tectonophysics, v. 190, p. 209–232, doi: 10.1016/0040-1951(91)90431-Q.

Jennings, C.W., 1977, Geologic Map of California: California Division of Mines and Geology, Geologic Data Map 2, scale 1:750,000.

Jolivet, M., Brunel, M., Seward, D., Xu, Z., Yang, J., Roger, F., Tapponnier, P., Malavieille, J., Arnaud, N., and Wu, C., 2001, Mesozoic and Cenozoic tectonics of the northern edge of the Tibetan Plateau; fission-track constraints: Tectonophysics, p. 111–134.

Keller, J.V.A., Hall, S.H., and McClay, K.R., 1997, Shear fracture pattern and microstructural evolution in transpressional fault zones from field and laboratory studies: Journal of Structural Geology, v. 19, no. 9, p. 1173–1187, doi: 10.1016/S0191-8141(97)00042-4.

Kendrick, K.J., Morton, D.M., Wells, S.G., and Simpson, R.W., 2002, Spatial and temporal deformation along the northern San Jacinto fault, southern California: Implications for slip rates: Bulletin of the Seismological Society of America, v. 92, no. 7, p. 2782–2802.

Krantz, R.W., 1995, The transpressional strain model applied to strike-slip, oblique-convergent, and oblique-divergent deformation: Journal of Structural Geology, v. 17, no. 8, p. 1125–1137, doi: 10.1016/0191-8141(94)00129-N.

Lee, K.Y., 1984, Geology of the Chaidamu basin, Qinghai Province, northwest China: U.S. Geological Survey Open-file Report 84-413, 46 p.

Lisowski, M., Prescott, W.H., Savage, J.C., and Johnston, M.J., 1989, Geodetic estimate of coseismic slip during the 1989 Loma Prieta, California earthquake: Geophysical Research Letters, v. 17, p. 1437–1440.

Liu, L., and Zoback, M.D., 1992, The effect of topography on the state of stress in the crust: application to the site of the Cajon Pass scientific drilling project: Journal of Geophysical Research, v. 97, no. B4, p. 5095–5108.

Liu, Z.Q., 1988, Geologic Map of the Qinghai-Xizang Plateau and its Neighboring Regions (in Chinese): Chengdu Institute of Geology and Mineral Resources, Academica Sinica Geology Publisher, scale 1:1,500,000.

Ma, X., 1980, Lithospheric Dynamics Map of China and Adjacent Seas: Geological Publishing House, scale 1:4,000,000.

McClay, K., and Bonora, M., 2001, Analog models of restraining stepovers in strike-slip fault systems: AAPG Bulletin, v. 85, no. 2, p. 233–260.

McKenzie, D., Nimmo, F., Jackson, J.A., Gans, P.B., and Miller, E.L., 2000, Characteristics and consequences of flow in the lower crust: Journal of Geophysical Research, v. 105, no. B5, p. 11,029–11,046, doi: 10.1029/1999JB900446.

McTigue, D.F., and Mei, C.C., 1981, Gravity-induced stresses near topography of small slope: Journal of Geophysical Research, v. 86, no. B10, p. 9,268–9,278.

Medwedeff, D.A., 1989, Growth fault-bend folding at southeast Lost Hills, San Joaquin Valley, California: American Association of Petroleum Geologists Bulletin, v. 73, no. 1, p. 54–67.

Medwedeff, D.A., 1992, Geometry and kinematics of an active, laterally propagating wedge thrust, Wheeler Ridge, California, *in* Mitra, S., and Fisher, G.W., eds., Structural Geology of Fold and Thrust Belts: Baltimore, Johns Hopkins University Press, p. 3–28.

Meriaux, A.S., Tapponnier, P., Ryerson, F.J., Van der Woerd, J., King, G., Meyer, B., Finkel, R., and Caffee, M., 1997, Application of cosmogenic 10Be and 26Al dating to neotectonics of the Altyn Tagh fault in central Asia (Gansu, China): EOS, Transactions, American Geophysical Union, v. 78, no. 46, p. F173.

Meriaux, A.S., Ryerson, F.J., Tapponnier, P., Van der Woerd, J., Lasserre, C., and Xu, X., 1998, Large-scale strain patterns, great earthquakes, and Late Pleistocene slip-rate along the Altyn Tagh fault (China): EOS, Transactions, American Geophysical Union, v. 79, no. 45, p. F190.

Meriaux, A.S., Ryerson, F.J., Tapponnier, P., Van der Woerd, J., Finkel, R.C., Caffee, M.W., Lasserre, C., Xu, X., Li, H., and Xu, Z., 2000, Fast extrusion of the Tibet Plateau: a 3cm/yr, 100Kyr slip-rate on the Altyn Tagh fault: EOS, Transactions, American Geophysical Union, v. 81, no. 48, p. F1137.

Métivier, F., Gaudemer, Y., Tapponnier, P., and Meyer, B., 1998, Northeastward growth of the Tibetan plateau deduced from balanced reconstruction of two depositional areas: the Qaidam and Hexi Corridor basins, China: Tectonics, v. 17, no. 6, p. 823–842, doi: 10.1029/98TC02764.

Meyer, B., Tapponnier, P., Bourjot, L., Metivier, F., Gaudemer, Y., Peltzer, G., Guo, S., and Chen, Z., 1998, Crustal thickening in Gansu-Qinghai, lithospheric mantle subduction, and oblique, strike-slip controlled growth of the Tibet plateau: Geophysical Journal International, v. 135, p. 1–47, doi: 10.1046/J.1365-246X.1998.00567.X.

Molnar, P., and Lyon-Caen, H., 1988, Some simple physical aspects of the support, structure, and evolution of mountain belts, *in* Clark, S.P., Burchfiel, B.C., and Suppe, J., eds., Processes in Continental Lithospheric Deformation: Geological Society of America Special Paper 218, p. 179–207.

Molnar, P., and Tapponnier, P., 1975, Cenozoic tectonics of Asia; effects of a continental collision: Science, v. 189, no. 4201, p. 419–426.

Molnar, P., and Tapponnier, P., 1978, Active tectonics of Tibet: Journal of Geophysical Research, v. 83, no. B11, p. 5361–5375.

Molnar, P., Burchfiel, B.C., K'uangyi, L., and Ziyun, Z., 1987a, Geomorphic evidence for active faulting in the Altyn Tagh and northern Tibet and qualitative estimates of its contribution to the convergence of India and Eurasia: Geology, v. 15, no. 3, p. 249–253.

Molnar, P., Burchfiel, B.C., Zhao, Z., Liang, K., Wang, S., and Huang, M., 1987b, Geologic evolution of northern Tibet: Results of an expedition to Ulugh Muztagh: Science, v. 235, p. 299–305.

Mount, V.S., and Suppe, J., 1987, State of stress near the San Andreas fault: implications for wrench tectonics: Geology, v. 15, p. 1143–1146.

Nielsen, S.B., and Knopoff, L., 1998, The equivalent strength of geometrical barriers to earthquakes: Journal of Geophysical Research-Solid Earth, v. 103, no. B5, p. 9953–9965, doi: 10.1029/97JB03293.

Owen, L.A., Cunningham, W.D., Windley, B.F., Badamgarov, J., and Dorjnamjaa, D., 1999, The landscape evolution of Nemegt Uul: a late Cenozoic transpressional uplift in the Gobi Altai, southern Mongolia, *in* Smith, B.J., Whalley, W.B., and Warke, P.A., eds., Uplift, Erosion and Stability: Perspectives on Long

Term Landscape Development: Geological Society [London] Special Publication 162, p. 201–218.
Paylor, E.J., II, and Yin, A., 1993, Left-slip evolution of the North Owl Creek fault system, Wyoming, during Laramide shortening: Geological Society of America Special Paper 280, p. 229–242.
Peltzer, G., and Tapponnier, P., 1988, Formation and evolution of strike-slip faults, rifts, and basins during the India-Asia collision: An experimental approach: Journal of Geophysical Research, v. 93, no. B12, p. 15,085–15,117.
Peltzer, G., Tapponnier, P., and Armijo, R., 1989, Magnitude of late Quaternary left-lateral movement along the north edge of Tibet: Science, v. 246, no. 4935, p. 1285–1289.
Petit, J.P., 1987, Criteria for the sense of movement on fault surfaces in brittle rocks: Journal of Structural Geology, v. 9, no. 5/6, p. 597–608.
Platt, J.P., Leggett, J.K., and Alam, S., 1988, Slip vectors and fault mechanics in the Makran accretionary wedge, southwest Pakistan: Journal of Geophysical Research, v. 93, no. B7, p. 7955–7973.
Richardson, R.M., and Coblentz, D.D., 1994, Stress modeling in the Andes: constraints on the South American intraplate stress magnitudes: Journal of Geophysical Research, v. 99, no. B11, p. 22,015–22,025, doi: 10.1029/94JB01751.
Ritts, B.D., and Biffi, U., 2000, Magnitude of post-Middle Jurassic (Bajocian) displacement on the Altyn Tagh fault system, northwest China: Geological Society of America Bulletin, v. 112, no. 1, p. 61–74, doi: 10.1130/0016-7606(2000)1122.3.CO;2.
Ron, H., 1987, Deformation along the Yammuneh, the restraining bend of the Dead Sea transform: paleomagnetic data and kinematic implications: Tectonics, v. 6, no. 5, p. 653–666.
Ron, H., Freund, R., and Garfunkel, Z., 1984, Block rotation by strike-slip faulting: structural and paleomagnetic evidence: Journal of Geophysical Research, v. 89, no. B7, p. 6256–6270.
Ron, H., Nur, A., and Eyal, Y., 1990, Multiple strike-slip fault sets: a case study from the Dead Sea transform: Tectonics, v. 9, no. 6, p. 1421–1431.
Royden, L., 1996, Coupling and decoupling of crust and mantle in convergent orogens: Implications for strain partitioning in the crust: Journal of Geophysical Research, v. 101, no. B8, p. 17,679–17,705, doi: 10.1029/96JB00951.
Rumelhart, P.E., 1998, Cenozoic basin evolution of southern Tarim, northwestern China: Implications for the uplift history of the Tibetan Plateau [Ph.D. thesis]: Los Angeles, University of California, 268 p.
Saucier, F., Humphreys, E., and Weldon, R., 1992, Stress near geometrically complex strike-slip faults: application to the San Andreas fault at Cajon Pass, Southern California: Journal of Geophysical Research, v. 97, no. B4, p. 5081–5094.
Savage, W.Z., and Swolfs, H.S., 1986, Tectonic and gravitational stress in long symmetric ridges and valleys: Journal of Geophysical Research, v. 91, no. B3, p. 3677–3685.
Scholz, C.H., 2000, Evidence for a strong San Andreas fault: Geology, v. 28, no. 2, p. 163–166, doi: 10.1130/0091-7613(2000)0282.3.CO;2.
Scholz, C.H., and Saucier, F.J., 1993, What Do the Cajon Pass Stress Measurements Say About Stress on the San-Andreas Fault—in-Situ Stress Measurements to 3.5 Km Depth in the Cajon Pass Scientific-Research Borehole—Implications for the Mechanics of Crustal Faulting—Comment: Journal of Geophysical Research-Solid Earth, v. 98, no. B10, p. 17,867–17,869.
Segall, P., and Pollard, D.D., 1980, Mechanics of discontinuous faults: Journal of Geophysical Research, v. 85, no. B10, p. 4337–4350.
Shen, Z.-K., Wang, M., Li, Y., Jackson, D.D., Yin, A., Dong, D., and Fang, P., 2001, Crustal deformation along the Altyn Tagh fault system, western China, from GPS: Journal of Geophysical Research, v. 106, no. B12, p. 30,607–30,621, doi: 10.1029/2001JB000349.
Sobel, E.R., Arnaud, N., Jolivet, M., Ritts, B.D., and Brunel, M., 2001, Jurassic to Cenozoic exhumation history of the Altyn Tagh range, northwest China, constrained by 40Ar/39Ar and apatite fission track thermochronology, *in* Hendrix, M.S., and Davis, G.A., eds., Paleozoic and Mesozoic Tectonic Evolution of Central and Eastern Asia: From Continental Assembly to Intracontinental Deformation: Boulder, Colorado, Geological Society of America Memoir 194, p. 247–267.
Spotila, J.A., and Sieh, K., 2000, Architecture of transpressional thrust faulting in the San Bernadino Mountains, southern California, from deformation of a deeply weathered surface: Tectonics, v. 19, no. 4, p. 589–615, doi: 10.1029/1999TC001150.
Spotila, J.A., Farley, K.A., and Sieh, K., 1998, Uplift and erosion of the San Bernardino Mountains associated with transpression along the San Andreas fault, California, as constrained by radiogenic helium thermochronometry: Tectonics, v. 17, no. 3, p. 360–378, doi: 10.1029/98TC00378.
Spotila, J.A., Farley, K.A., Yule, J.D., and Reiners, P.W., 2001, Near-field transpressive deformation along the San Andreas fault zone in southern California, based on exhumation constrained by (U-Th)/He dating: Journal of Geophysical Research, v. 106, no. B12, p. 30,909–30,922, doi: 10.1029/2001JB000348.
Sylvester, A.G., 1988, Strike-slip faults: Geological Society of America Bulletin, v. 100, p. 1666–1703, doi: 10.1130/0016-7606(1988)1002.3.CO;2.
Tapponnier, P., and Molnar, P., 1977, Active faulting and tectonics in China: Journal of Geophysical Research, v. 82, no. 20, p. 2,905–2,930.
Teyssier, C., and Tikoff, B., 1998, Strike-slip partitioned transpression of the San Andreas fault system: a lithospheric-scale approach, *in* Holdsworth, R.E., Strachan, R.A., and Dewey, J.F., eds., Continental Transpressional and Transtensional Tectonics: The Geological Society [London] Special Publication 135, p. 143–158.
Townend, J., and Zoback, M.D., 2000, How faulting keeps the crust strong: Geology, v. 28, no. 5, p. 399–402, doi: 10.1130/0091-7613(2000)0282.3.CO;2.
Turcotte, D.L., and Schubert, G., 1982, Geodynamics: New York, John Wiley and Sons, 450 p.
Twiss, R.J., and Unruh, J.R., 1998, Analysis of fault slip inversions: do they constrain stress or strain rate?: Journal of Geophysical Research, v. 103, no. B6, p. 12,205–12,222, doi: 10.1029/98JB00612.
Van der Woerd, J., Xu, X., Li, H., Tapponnier, P., Meyer, B., Ryerson, F.J., Meriaux, A.-S., and Xu, Z., 2001, Rapid active thrusting along the northwestern rangefront of the Tanghe Nan Shan (western Gansu, China): Journal of Geophysical Research, v. 106, no. B12, p. 30,475–30,504, doi: 10.1029/2001JB000583.
Walley, C.D., 1988, A braided strike-slip model for the northern continuation of the Dead Sea fault and its implications for Levantine tectonics: Tectonophysics, v. 145, p. 63–72, doi: 10.1016/0040-1951(88)90316-2.
Walley, C.D., 1998, Some outstanding issues in the geology of Lebanon and their importance in the tectonic evolution of the Levantine region: Tectonophysics, v. 298, p. 37–62, doi: 10.1016/S0040-1951(98)00177-2.
Washburn, Z., Arrowsmith, J.R., Dupont-Nivet, G., and Wang, X.-F., 2000, Earthquake geology of the Central Altyn Tagh fault from Lake Wuzhunxiao (38.4N, 89.9E) to Lapequan (39.1N, 92.5E), China: EOS, Transactions, American Geophysical Union, v. 81, no. 48, p. F1137.
Washburn, Z., Arrowsmith, J.R., Forman, S.L., Cowgill, E., Wang, X., Zhang, Y., and Chen, Z., 2001, Late Holocene earthquake history of the central Altyn Tagh Fault, China: Geology, v. 29, no. 11, p. 1051–1054, doi: 10.1130/0091-7613(2001)0292.0.CO;2.
Washburn, Z., Arrowsmith, J.R., DuPont-Nivet, G., Wang, X.-F., Zhang, Y.-Q., and Chen, Z., 2003, Earthquake Geology of the central Altyn Tagh Fault, Xinjiang, China: Annals of Geophysics, v. 46, no. 5, p. 1015–1034.
Wesnousky, S.G., 1988, Seismological and structural evolution of strike-slip faults: Nature, v. 335, p. 340–343, doi: 10.1038/335340A0.
Wessel, P., and Smith, W.H.F., 1991, Free software helps map and display data: EOS, Transactions, American Gephysical Union, v. 72, p. 441.
Westaway, R., 1995, Deformation around stepovers in strike-slip fault zones: Journal of Structural Geology, v. 17, no. 6, p. 831–846, doi: 10.1016/0191-8141(94)00098-K.
Wittlinger, G., Tapponnier, P., Poupinet, G., Jiang, M., Shi, D., Herquel, G., and Masson, F., 1998, Tomographic evidence for localized lithospheric shear along the Altyn Tagh fault: Science, v. 282, p. 74–76, doi: 10.1126/SCIENCE.282.5386.74.
Woodcock, N.H., and Fischer, M., 1986, Strike-slip duplexes: Journal of Structural Geology, v. 8, no. 7, p. 725–735, doi: 10.1016/0191-8141(86)90021-0.
Xinjiang Bureau of Geology and Mineral Resources, 1993, Regional Geology of Xinjiang Uygur Autonomous Region (in Chinese with English abstract), Geological Memoirs of the Ministry of Geology and Mineral Resources: Beijing, P.R. China, Geological Publishing House, 841 p.
Yin, A., and Harrison, T.M., 2000, Geologic Evolution of the Himalayan-Tibetan Orogen: Annual Review of Earth and Planetary Science, v. 28, p. 211–280, doi: 10.1146/ANNUREV.EARTH.28.1.211.
Yin, A., Rumelhart, P.E., Butler, R., Cowgill, E., Harrison, T.M., Foster, D.A., Ingersoll, R.V., Zhang, Q., Zhou, X.-Q., Wang, X.-F., Hanson, A., and Raza, A., 2002, Tectonic history of the Altyn Tagh fault system in northern Tibet inferred from Cenozoic sedimentation: Geological Society of America Bulletin, v. 114, no. 10, p. 1257–1295, doi: 10.1130/0016-7606(2002)1142.0.CO;2.
Yue, Y., Ritts, B.D., and Graham, S.A., 2001, Initiation and long-term slip history of the Altyn Tagh fault: International Geology Review, v. 43, p. 1087–1093.
Zachariasen, J., and Sieh, K., 1995, The transfer of slip between two en echelon strike-slip faults: a case study from the 1992 Landers earthquake, southern California: Journal of Geophysical Research, v. 100, no. B8, p. 15,281–15,301, doi: 10.1029/95JB00918.
Zheng, J., 1991, Significance of the Altun Tagh fault of China: Episodes, v. 14, no. 4, p. 307–312.
Zheng, J., 1994, Geodynamics of Altun Tagh fault: Journal of China University of Geosciences, v. 5, no. 1, p. 41–45.
Zoback, M.D., Zoback, M.L., Mount, V.S., Suppe, J., Eaton, J.P., Healy, J.H., Oppenheimer, D., Reasenberg, P., Jones, L., Raleigh, C.B., Wong, I.G., Scotti, O., and Wentworth, C., 1987, New evidence on the state of stress of the San Andreas fault system: Science, v. 238, p. 1105–1111.

Manuscript Received by the Society 20 March 2003
Revised Manuscript Received 3 January 2004
Manuscript Accepted 23 February 2004

Printed in the USA